(A New Proposal to Jefferson Lab 12 GeV -PAC32)

Large Acceptance Proton Form Factor Ratio Measurements at 13 and 15 $(GeV/c)^2$ Using Recoil Polarization Method

C.F. Perdrisat (spokesperson), L.P. Pentchev (spokesperson-contact),
D. Armstrong, T. Averett, R. Feuerbach, M. Finn, M. Meziane
College of William and Mary

E. Cisbani(spokesperson), F. Cusanno, F. Garibaldi,
S. Frullani, G. M. Urciuoli, M. Iodice, M.L. Magliozzi
INFN, Rome, Italy

V. Punjabi (spokesperson), M. Khandaker, F. Wesselmann
Norfolk State University

B. Wojtsekhowski (spokesperson), A. Camsonne, J.P. Chen,
E. Chudakov, C. DeJager, H. Fenker, P. Degtyarenko, M. Jones, J. Gomez,
O. Hansen, D. W. Higinbotham, J. LeRose, R. Michaels, S. Nanda, A. Saha
Thomas Jefferson National Accelerator Facility, Newport News, VA 23606

E. Brash and D. Doughty
Christopher Newport University, Newport News, VA and
Thomas Jefferson National Accelerator Facility, Newport News, VA 23606

E. Tomasi-Gustafsson
DAPNIA, Saclay, France

W. Boeglin, P. Markowitz, J. Reinhold
Florida International University, Fl

V.P. Kubarovsky, A. Davidenko, Yu.M. Goncharenko, A.P. Meschanin,
Yu.M. Melnik, L.F. Soloviev and A.N. Vasiliev
Institut for High Energy Physics, Protvino, Russia

N. Piskunov, D. Kirillov, I. Sitnik
Laboratory for High Energy, JINR, Dubna, Russia

G. Cates, D. Day, R. Lindgren, N. Liyanage,
V. Nelyubin, B. Norum, K. Paschke
University of Virginia, Charlottesville, VA 22901

J. Annand, D. Ireland, R. Kaiser, K. Livingston,
I. MacGregor, B. Seitz, and G. Rosner
University of Glasgow, Glasgow, Scotland

W. Bertozzi, S. Gilad, J. Huang, B. Moffit,
P. Monaghan, N. Muangma, A. Puckett, X. Zhan
Massachusetts Institute of Technology, Cambridge, MA 02139

D. Nikolenko, I. Rachek, Yu. Shestakov
Budker Institute, Novosibirsk, Russia

G.B. Franklin, B. Quinn
Carnegie Mellon University, Pittsburgh, PA 15213

R. De Leo, L. La Gamba, S. Marrone, E. Nappi
INFN, Bari, Italy

C.E. Hyde^{+} and A. Radyushkin
Old Dominion University, Norfolk, VA 23529
$^{+}$ *also Laboratoire de Physique Corpusculaire,*
Universit Blaise Pascal, 63177 Aubire FRANCE

E. Piasetzky, G. Ron, J. Lichtenstandt
Tel Aviv University, Israel

R. Wilson
Harvard University, Cambridge, MA 02138

A. Glamazdin
Kharkov Institute of Physics and Technology, Kharkov 310077, Ukraine

J. Calarco
University of New Hampshire, Durham, NH 03824

B. Vlahovic
North Carolina Central University, Durham, NC 03824

A. Sarty
Saint Mary's University, Nova Scotia, Canada B3H 3C3

G. Huber
University of Regina, Regina, Canada S4S 0A2

Piotr Decowski
Smith College, Northampton, MA 01063

S. Nedev
University of Chemical Technology, Sofia, Bulgaria

K. Aniol and D. J. Magaziotis
Cal State University, Los Angeles, CA 90032

S. Abrahamyan, A. Ketikyan, S. Mayilyan, A. Shahinyan, H. Voskanyan
Yerevan Physics Institute, Yerevan, Armenia

June 21, 2007

1 Abstract

The polarization transfer technique was successfully used in the high precision measurements of the proton elastic form factor ratio G_{Ep}/G_{Mp} at JLab in two experiments in Hall A. In the first (E93-027), a maximum Q^2 of 3.5 GeV^2 was obtained, and in the second (E99-007) a Q^2 of 5.6 was reached. The forthcoming experiment in Hall C (E04-108) will extend these measurements to 9 GeV^2, close to the limit for a 6 GeV beam. Increasing the beam energy to 11 GeV will push the limit of these measurements to a Q^2 of 15 GeV^2 or higher.

In this proposal we demonstrate that using a single dipole detector system with large solid angle, which includes a polarimeter and a hadron calorimeter, to detect the recoil proton, we can obtain good statistical error bars up to a Q^2 of $\sim$ 15 GeV^2.

As in experiment E-04-108, GEp(3), the scattered electron will be detected in the lead glass calorimeter BigCal, which allows for solid angle matching for all kinematics proposed. The tracking part of the proton arm will consist of three gas electron multiplier (GEM) detectors, each consisting of 3 planes. The high fluxes of charged- and neutral particles that these detectors can sustain make it possible to design an experiment with small bending angle in the dipole and to have the front detector in direct view of the target.

This experiment will extend the range of Q^2 significantly, with statistical and systematic uncertainties similar to the first three G_{Ep}/G_{Mp} experiments. The anticipated results will provide a definitive test of the many phenomenological models at high Q^2, which do describe the present data base.

Contents

2 Collaboration contributions to 12 GeV baseline equipment

There are four items listed under Hall A 12 GeV baseline equipment:

- arc energy measurement system,
- the Compton polarimeter,
- the Møller polarimeter,
- the HRS readout electronics.

Two of these items are essential for the proposed experiment: Compton polarimeter for continuous monitoring of the beam polarization and Møller polarimeter for the planned spin "dance".

The collaboration **intends** to contribute to the development of the HRS readout electronics and associated software. This collaboration **intends** to make major contributions to the **commissioning of Compton and Møller polarimeters**.

The spokespeople of this experiment include members of two university groups that have played a major role in the Hall A physics program and a large research group from INFN, which has made major contributions to the development of high-tech detectors, and motivated innovative experiments. These groups have made significant contributions to the base equipment in Hall A from the beginning; these include commissioning of the Hall A high resolution spectrometer pair, development of the septum magnets and a state-of-the art particle identification RICH detector, and design, construction and commissioning of the Hall A focal plane polarimeter used in many experiments.

In addition, one of the PIs of this proposal is leading a collaboration of 4 Universities which will build, install and calibrate the standard **detector package for the Hall C super HMS**. An MRI proposal to NSF has been submitted and will be funded.

The magnet-detector setup this collaboration is proposing to build and commission will be a valuable device for many future experiments in Hall A with the upgraded 11 GeV beam.

3 Introduction

An experiment is proposed, to measure the ratio of the proton elastic form factors, G_{Ep} and G_{Mp}, to 15 GeV^2, using the recoil polarization technique. To obtain sufficient statistics for such large momentum transfer the recoil proton will be detected in a new detector which will include a single dipole magnet, a polarimeter with three sets of tracking chambers, and a hadron calorimeter. The dipole is available from the fixed target AGS program at BNL. For the hadron calorimeter there are several options. One likely option is to reuse parts of calorimeters that exist at several collaborating institutions. The new and key part of the detector, for which in this experiment an international collaboration is built up, is a set of tracking chambers, which are conceptually similar to ones used in the COMPASS experiment at CERN.
The dipole will bend positively charged particles upwards, the elastically scattered recoil protons by 6 degrees, and background charged particles will be swept out of the tracking detectors. The proton spin will precess by optimum angle of 90°. A trigger in the hadron calorimeter will have a high threshold of 4 GeV. A track of the proton will be recorded three times: first in the tracker after the dipole magnet, second after the 50 cm CH_2 block and the third after a second 50 cm CH_2 block. The scattered electron will be detected in coincidence in the recently built lead glass calorimeter BigCal, which has good energy and position resolution. The new data will give access to a region of Q^2 in which G_{Ep} is completely unknown; it corresponds to very short distances inside the proton, a kinematical region most critical for the testing of QCD based models of the nucleon.

The structure of the proton (and of the neutron), as revealed by elastic electron scattering, has been investigated experimentally and theoretically for over 50 years. Form factor data are of great interest as a testing ground for QCD, as results from lattice QCD calculations become increasingly accurate and realistic. Phenomenological models have recently been challenged by elastic form factors obtained at Jefferson Lab, resulting in an intense discussion of questions related to the shape of the proton [1, 2], and the contribution of the quark orbital angular momentum to its spin, for example [3].

The two Sachs form factors, G_{Ep} and G_{Mp}, required to describe the nucleon charge- and magnetization distribution have been traditionally obtained by Rosenbluth separation. The G_{Mp}-data obtained by this method have shown good internal consistency up to 30 GeV^2. However, the characterization of G_{Ep} has suffered from large inconsistencies in the data base, which are now understood to be the result of the fast decrease of the contribution of G_{Ep} to the cross section.

An entirely new picture of the structure of the proton has emerged after two experiments in Hall A showed that the ratio G_{Ep}/G_{Mp} was in fact not constant, and decreased by a factor of 3.7 over the Q^2 range of 1 to 5.6 GeV^2. These results are illustrated in Fig. 1, and are also compared with Rosenbluth separation data.

Following the unexpected results from the polarization experiments, a new experiment

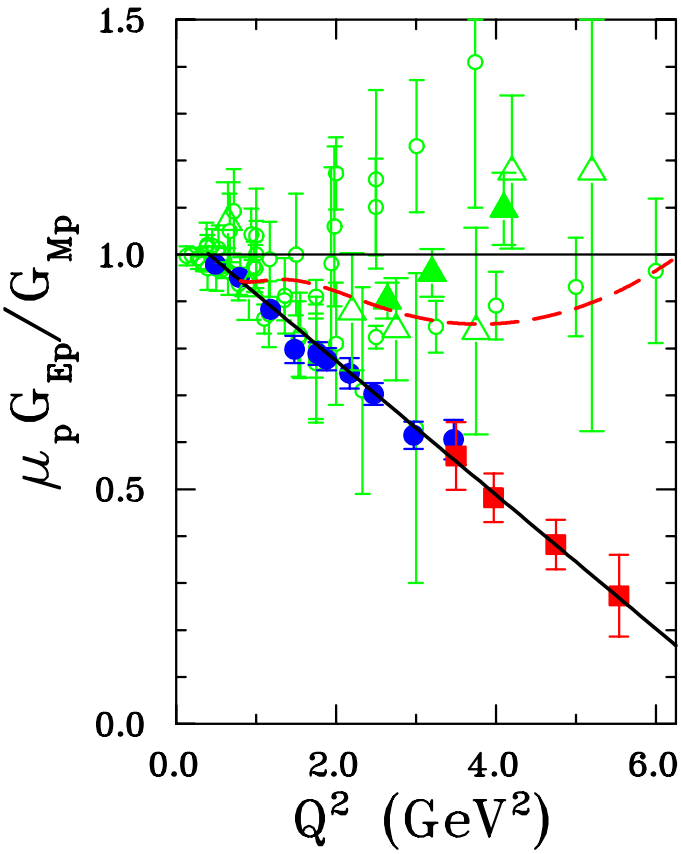

Figure 1: Comparison of $\mu_p G_{Ep}/G_{Mp}$ from the two JLab polarization data [5, 6], and Rosenbluth separation; dashed curve is a re-fit of Rosenbluth data [7]; solid curve is an updated form of the fit in ref. [8].

was approved, to extend the Q^2-range to 9 GeV^2 in Hall C. This experiment will start taking data in the Fall of 2007. Possible beam energy limitations might lower the largest Q^2-value to 8.5 GeV^2. In this forthcoming experiment the recoil proton will be detected in the HMS equipped with a new double focal plane polarimeter. The scattered electron will be detected in a new lead glass calorimeter (BigCal) built for this purpose out of 1744 glass bars, 4x4 cm^2 each, giving a total frontal area of 2.6 m^2, which provides complete kinematical matching.

A letter of intent was submitted to PAC 30, to continue using this technique up to Q^2=13 GeV^2 when an 11 GeV beam becomes available, by installing a the new double polarimeter setup in the new super HMS to be built in Hall C, and again detecting the electron in BigCal. This experiment is rate limited by the small acceptance of the SHMS, but uses a proven technique and will require no new equipment, besides what is planned for Hall C at 12 GeV. A full proposal will be submitted to PAC34 (GEP(4)).

It is well known by now that G_{Ep} is difficult to obtain from Rosenbluth separation, a technique which is also especially sensitive to systematics errors and subject to large, ϵ-dependent radiative corrections. The two-photon exchange contribution, neglected in the past, has been shown to be an important term to add to the standard radiative corrections

for cross section data; it has a strong ϵ-dependence and brings the Rosenbluth form factor ratio closer to the recoil polarization results. Two-photon contributions are expected to affect the recoil polarization results only very weakly. Fig. 2 shows a prediction ([4]) for the correction to $\mu G_{Ep}/G_{Mp}$ as a function of Q^2 and ϵ; according to this calculation the correction remains small up to the large Q^2 of this proposal.

The recoil polarization data have very different and easily tractable sources of systematics uncertainty than the Rosenbluth data, the dominant one being the spin transport throughout the magnetic system of the proton detector. Techniques to correct for spin precession in various magnetic detectors have been perfected in the hall A experiments; no difficulties related to spin transport are expected in the new detector system proposed below.

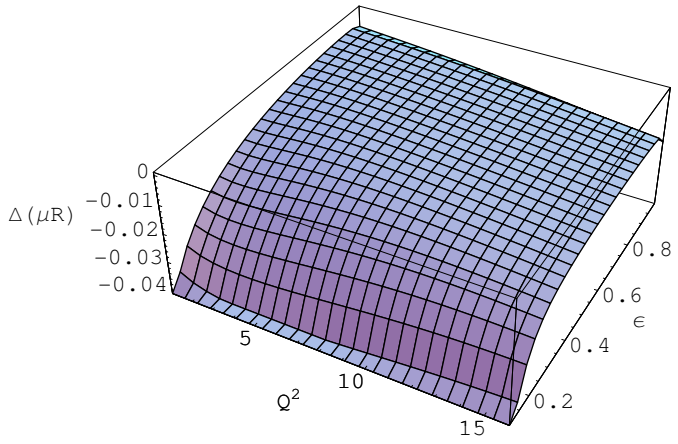

Figure 2: A prediction from Afanasev et al. [4] for the correction to the $\mu_p G_{Ep}/G_{Mp}$ ratio obtained in recoil polarization experiments, due to two hard photon exchange, versus Q^2 and ϵ.

The results from the two previous recoil polarization experiments have been one of the most quoted and most publicized JLab accomplishments to date.

The meaning of the results seen in Fig. 1 is that the spatial distribution of the electric charge of the proton is "softer", i.e. larger in extent (in the Breit frame), than its magnetic moment distribution, which is definitively not intuitive. However, the relativistic boost required to transform these spatial distributions back to the laboratory frame are not trivial and only the form factors themselves are relativistic invariants. Recently G.A. Miller [9] has shown that an invariant charge distribution can only be defined on the wave front; the two-dimensional charge density on the wave front is the Fourier transform of the Dirac form factor, F_1.

The decrease of the G_{Ep}/G_{Mp} ratio had been predicted years before the experiments actually occurred (for example Iachello, Miller, Holzwarth). The experimental results also suggest that the ratio of the Pauli to Dirac form factor does not even begin to approach the asymptotic limit predicted by pQCD, which would be signaled by Q^2F_2/F_1 becoming

constant; Fig. 2 illustrates this point. Based on the currently available data suggest that the G_{Ep}/G_{Mp} ratio will cross zero near 8 GeV^2. Experiments using a 11 GeV beam might therefore explore the region of Q^2 where the ratio is negative.

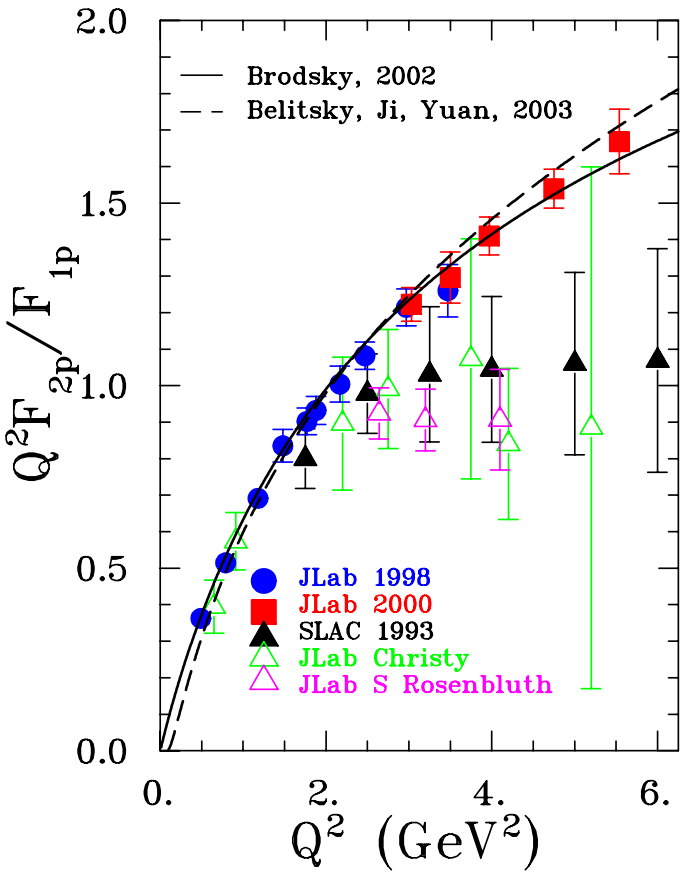

Figure 3: The ratio F_{2p}/F_{1p}, obtained directly from the recoil polarization ratio G_{Ep}/G_{Mp}, and multiplied by Q^2; the Rosenbluth data of refs. [10, 11, 12] are also shown.

The present proposal, GEP(5), breaks away from the tested technique of detecting the proton in a high- or medium resolution magnetic spectrometer equipped with a focal plane polarimeter, with necessarily small solid angle. Instead, a single dipole with very large acceptance and solid angle bending the elastic recoil proton vertically, with favorable precession angle of the longitudinal polarization component, and sweeping the low energy part of the charged background particles away from the front tracker, will be used. This concept trades high resolution and small solid angle for low resolution and large solid angle, an advantage when the laboratory differential cross section drops as E^2_{beam}/Q^{12}. This configuration can potentially reach larger Q^{2}s because of the larger acceptance, but is limited to one configuration which covers the Q^2 range 12.3 to 16 GeV^2 in one setting. The data will then be divided into two parts, with central values of Q^2 of 12.9 and 14.75 GeV^2, respectively. The absolute statistical uncertainties for these two points, $\Delta(G_{Ep}/G_{Mp})$, are expected to be 0.088 and 0.105, respectively.

The proposed new detector for the recoil proton includes a front tracker close behind the dipole magnet, and consists of three GEM detectors, each with x,u,y coordinate readout to define the incoming proton angle and the interaction point at the target. This is followed by a double polarimeter of the type developed for GEP(3), but with two gas electron multiplier (GEM) detectors, instead of the two sets of drift chambers, each with three coordinate readouts.

The cost of the resolution/solid angle trade off is of course large background and high trigger rate. Solutions to this problem are addressed in the proposal, in which it will be shown that unwanted pions can be eliminated by using a hadron calorimeter on the proton side, downstream of the polarimeter. With a threshold set up high enough, the trigger rate can be decreased to modest and easily manageable levels. Also, the tracking in the front proton tracker and in the two polarimeter trackers will be greatly facilitated by the localization of the high energy component of the shower in the hadron calorimeter, as well as, by correlating the hadron track with the electron hit postion in the electromagnetic calorimeter.

4 Physics Motivation

The nucleon form factors contain information on the structure of a strongly interacting many-body system of quarks and gluons. Many theoretical attempts have been made to understand the nucleon form factors in terms of Quantum Chromodynamics (QCD). This reflects the fact that a direct calculation of nucleon form factors from the underlying theory of QCD, is extremely complicated as it requires, in the few GeV momentum transfer region, non-perturbative methods. Hence, in practice all theoretical models of the nucleon form factors involves approximations which often have a limited range of applicability. Despite their approximations and limitations, some of these non-perturbative methods do reveal some insight in the nucleon structure.

There are a number of different approaches to calculate nucleon form factors. The earliest models to explain the global features of the nucleon form factors, such as approximate dipole behavior, were vector meson dominance (VMD) models [13, 14, 15, 16, 17, 18, 19, 20, 21]. In this picture the photon couples to the nucleon through the exchange of vector mesons.

In the soliton model Holzwarth [22] applied the relativistic corrections due to recoil and incorporated partial coupling to vector mesons. He used the skyrmion as an extended object with one vector meson propagator and a relativistic boost to the Breit frame.

To understand the structure of the nucleon in terms of quark and gluon degrees of freedom, constituent quark models (CQM) have a long history. In QCD based models the photon couples to the quarks directly. To calculate the form factors of a system with small constituent masses and for momentum transfers several times the nucleon mass squared, a relativistic description becomes crucial. Many relativistic constituent quark models have been investigated [23, 24, 25, 26, 27, 28, 29, 30, 31] to calculate nucleon form factors. Other quark models that predict nucleon form factors include the cloudy bag model [32], di-quark model [33, 34], and QCD sum rules [35].

Lattice QCD simulations have the potential to calculate nucleon form factors from first principles [36, 37, 38, 39] . This is a rapidly developing field and important progress has been made in the recent past. Nevertheless, the lattice calculations are at present still severely limited by available computing power and in practice are performed for quark masses sizably larger than their values in nature. In contrast to all the models discussed above, lattice QCD currently offers the best prospects for computing nucleon form factors from first principles.

Generalized parton distributions (GPDs) are being accessed in hard exclusive reactions, which allow to remove in a controlled way a quark from the initial nucleon and re-implanting it in the final nucleon [40, 41, 42, 43, 44, 45, 46]. The resulting GPDs can be interpreted as quark correlation functions and have the property that their first moments exactly coincide with the nucleon form factors. Precise measurements of elastic nucleon form factors provide stringent constraints on the parameterization of the GPDs.

Perturbative QCD (pQCD) makes rigorous predictions when the four-momentum transfer squared, Q^2, is very large and the quarks become asymptotically free [47]. In this limit, the nucleon form factors describes a hard photon interacting with a valence quark in the nucleon, which then shares the momentum with the other (near collinear) valence quarks through gluon exchange [48, 49, 50, 51].

The starting point in understanding the interaction of a vector probe such as the photon

with a hadronic system is provided by the observation that the lowest lying hadrons with vector quantum numbers are the vector mesons $\rho(770)$, $\omega(782)$ and $\phi(1020)$. The number of mesons involved in the interaction and the coupling constants and masses of the mesons can be varied to fit the data.

Within such VMD models, the approximate dipole behavior of the nucleon electromagnetic form factors, $G_D = \frac{1}{(1+Q^2/0.71 GeV^2)^2}$, can be understood as being due to the contribution of two nearby vector meson poles which have opposite residua. Assume that one considers two vector meson pole contributions with masses m_{V1} and m_{V2}, and residua of equal magnitude and opposite sign a and $-a$ respectively, and one obtains :

$$F_{1,2}(q^2) \sim \frac{a}{q^2 - m_{V1}^2} + \frac{(-a)}{q^2 - m_{V2}^2} = \frac{a\,(m_{V1}^2 - m_{V2}^2)}{(q^2 - m_{V1}^2)(q^2 - m_{V2}^2)}. \quad (1)$$

An early VMD fit performed by Iachello *et al.* [13] predicted a linear decrease of the proton G_{Ep}/G_{Mp} ratio, in basic agreement with the result from the polarization transfer experiments. Such VMD models have been extended by Gari and Krümpelmann [15] to include the perturbative QCD (pQCD) scaling relations for the nucleon electromagnetic form factors.

In recent years, extended VMD fits have been obtained with a relatively good parameterization of all electromagnetic nucleon form factors. An example is Lomon's fit [18], which uses $\rho(770)$, $\omega(782)$, $\phi(1020)$, and $\rho'(1450)$ mesons and contains 11 parameters. Another such recent parameterization by Bijker and Iachello [20] include $\rho(770)$, $\omega(782)$, and $\phi(1020)$ mesons, but achieves a good fit by adding a phenomenological contribution attributed to a quark-like intrinsic qqq structure. The pQCD scaling relations are built into this fit which has 6 free parameters and fit the data. In contrast to the early fit of Ref. [13], the new fit of Ref. [20] gives a very good description of the neutron data at the expense of a slightly worse fit for the proton data.

The VMD model of Mergell *et al.* [16] is an expansion of the original work of Höhler *et al.* [14]. This analysis of nucleon electro magnetic form factors has been further improved by Belushkin *et al.* [21]. The parameters in their fit were constrained to yield the correct normalization of the form factors at zero momentum transfers. The asymptotic constraints from pQCD were included in two different forms : either as a super-convergence relation or by adding an explicit continuum term with the imposed pQCD behavior. A simultaneous fit to the world data for all four form factors in both the space-like and time-like regions was performed. Figure 4 shows this fit for the nucleon space-like form factors. It will be interesting to compare the most recent and sophisticated dispersion relation fit of [21] with data for G_{Ep}/G_{Mp} out to large Q^2 values.

The non-relativistic CQM, despite its simplicity, is quite successful in predicting the spectrum of low-lying baryons [53], and gives a relatively good description of static properties such as the octet baryon magnetic moments. However, to calculate the form factors, it is necessary to include relativistic effects because the momentum transfers involved are up to 10 times larger than the constituent quark mass.

In the earliest study of the relativistic constituent quark models (RCQM), Chung and Coester [23] calculated electromagnetic nucleon form factors using the light-front-form wave function with Poincaré-covariant constituent-quark models and investigated the effect of the

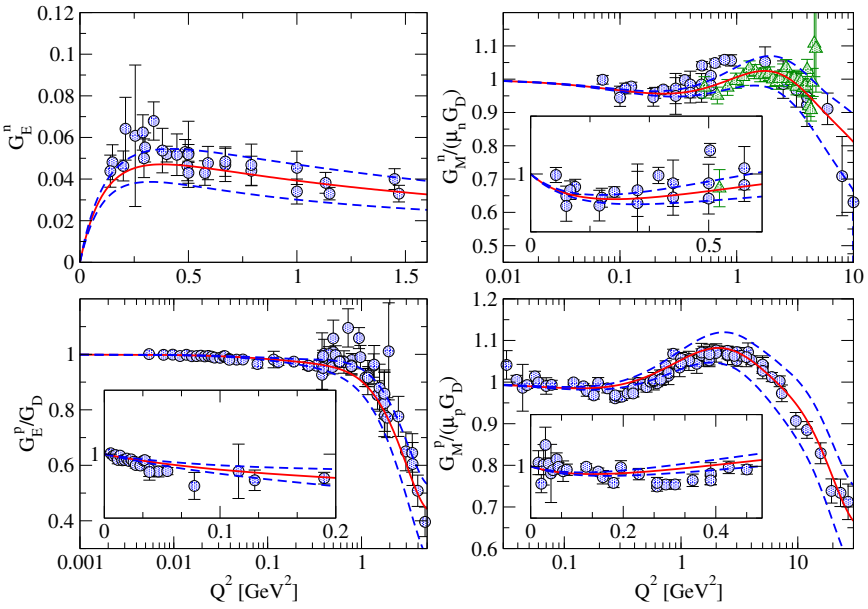

Figure 4: Dispersion relation (15 parameter) fit (solid curves) for the four nucleon (space-like) electromagnetic form factors compared with the world data (circles) including the JLab/CLAS data for G_{Mn} (triangles) [52]. The dashed curves indicate the 1σ deviation from the fit. Reprinted with permission from Ref. [21]. Copyright 2007 by the American Physical Society.

constituent quark masses, the anomalous magnetic moment of the quarks, and the confinement scale parameter. In Ref. [23] a Gaussian wave function fot the quark internal (transverse) momentum variables was used. Although this model yields a surprisingly good agreement with the observed G_{Ep}/G_{Mp} ratio, see Fig. 5, it yields nucleon form factors which drop too fast at larger Q^2 values when using constituent quark masses around 330 MeV.

The phenomenological light-front wave function of Schlumpf [54] was used by Frank, Jennings, and Miller [26, 55] to calculate the form factors. They showed that using a light-front wave function one cannot expect the pQCD prediction of hadron helicity conservation to apply and instead one finds that F_{2p}/F_{1p} drops less fast than $1/Q^2$ [55] in agreement with the G_{Ep}/G_{Mp} recoil polarization data [56, 5, 6].

Cardarelli *et al.* [27, 57] calculated the ratio with light-front dynamics and investigated the effects of SU(6) symmetry breaking. They showed that the decrease in the ratio with increasing Q^2 is due to the relativistic effects generated by Melosh rotations of the constituent quark's spins.

De Sanctis *et al.* [28] have calculated the ratio G_{Ep}/G_{Mp} within the hypercentral constituent quark model including relativistic corrections: however, the slope of their G_{Ep}/G_{Mp} ratio is too small by a factor of about two.

The chiral constituent quark model based on Goldstone-boson-exchange dynamics was used by Boffi *et al.* [29] to describe the elastic electromagnetic and weak form factors. They compute these form factors in a covariant framework using the point-form approach to relativistic quantum mechanics.

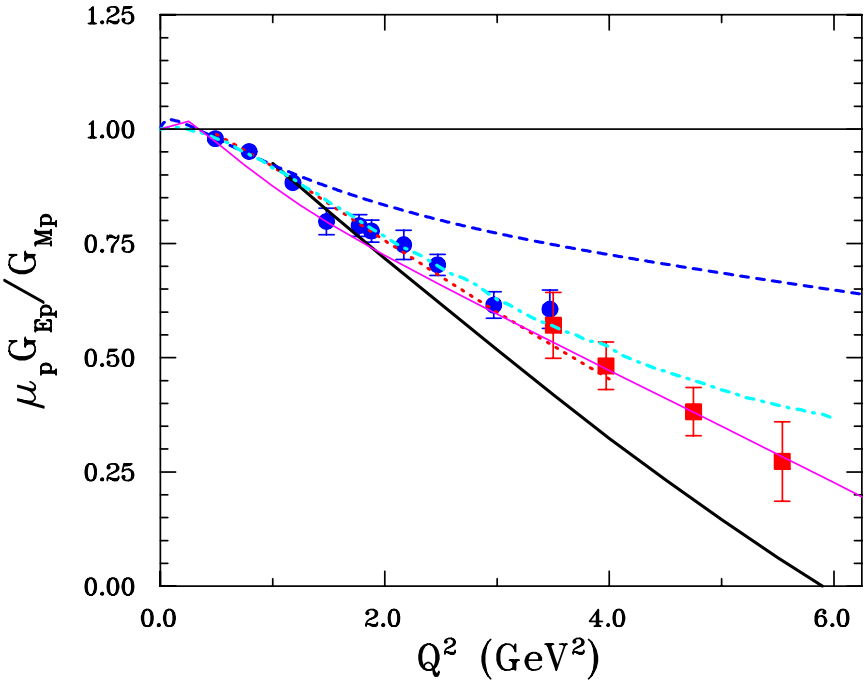

Figure 5: Comparison of relativistic constituent quark model calculations with the data for the ratio $\mu_p G_{Ep}/G_{Mp}$. Dotted curve : front form calculation of Chung and Coester [23] with point-like constituent quarks; thick solid curve : front form calculation of Frank *et al.* [26]; dot-dashed curve : front form calculation of Cardarelli *et al.* [27, 57] with point-like constituent quarks; dashed curve : point form calculation of Boffi et al. [29] in the Goldstone boson exchange model with point-like constituent quarks; thin solid curve : covariant spectator model of Gross and Agbakpe [30]. The data are from Refs. [6] (blue circles) and [5] (red squares).

More recently another covariant constituent quark model calculation was performed by Gross and Agbakpe [30], using a covariant spectator model. Assuming a simple pure S-wave form for the nucleon three-quark wave function, evaluating the current matrix element in a relativistic impulse approximation, and assuming constituent quark form factors including a phenomenological term which parameterizes the pion cloud, an eleven parameter description of the nucleon form factor data was obtained, see Fig. 5.

GPDs coincide with quark distribution functions at vanishing momentum transfer, and have links with other nucleon structure quantities. The first moments of the GPDs are related to the elastic form factors of the nucleon through model independent sum rules. The following relations for a particular quark flavor [3] hold true :

$$\int_{-1}^{+1} dx\, H^q(x,\xi,Q^2) \;=\; F_1^q(Q^2)\,, \qquad\qquad \int_{-1}^{+1} dx\, E^q(x,\xi,Q^2) \;=\; F_2^q(Q^2)\,, \tag{2}$$

where $F_1^q(Q^2)$ represents the elastic Dirac form factor for the quark flavor q in the nucleon. These quark form factors are expressed, using $SU(2)$ isospin, as flavor combinations of the

proton and neutron elastic form factors as:

$$F_1^u \,=\, 2\,F_{1p} \,+\, F_{1n}\;, \qquad\qquad F_1^d \,=\, 2\,F_{1n} \,+\, F_{1p}\,;\,, \tag{3}$$

where, neglecting the strange quark contribution, F_{1p} (F_{1n}) are the proton (neutron) Dirac form factors respectively.

Ref. [43] used a parameterization motivated from the expected Regge behavior of the GPDs at small x and Q^2. This yields to the ansatz R1 for the valence part of the GPD H^q :

$$H^q_{R1}(x,0,Q^2) = q_v(x)\,x^{\alpha' Q^2}, \tag{4}$$

where $q_v(x)$ is the forward valence quark distribution and α' is the slope of the corresponding Regge trajectory; a similar form is used for E^q_{R1}.

A modified Regge parametrization (R2 model) for the GPD E^q has been used by [58]:

$$E^q_{R2}(x,0,Q^2) \;\;=\;\; \frac{\kappa^q}{N^q}\,(1-x)^{\eta^q}\,q_v(x)\,x^{\alpha'\,(1-x)\,Q^2}\,. \tag{5}$$

The resulting Regge ansatz R2 has three free parameters which are to be determined from a fit to the form factor data.

In Figure 6, the results of the 1-parameter Regge model R1 is shown, with the value α' = 1.105 GeV^{-2}, which gives a good description of the proton charge radius. Obviously the Regge model R1 is able to reproduce the main trends of the proton electromagnetic form factor data for $Q^2 \leq 0.5$ GeV^2. The Regge model R2 is able to describe existing data at larger Q^2 with relatively good accuracy,with two additional parameters η^u and η^d. The GPD parameterization R2 also leads to a zero for G_{Ep} at a momentum transfer of $Q^2 \simeq 8$ GeV^2, which will be within the range covered by the upcoming JLab GEP(3) experiment [59].

The nucleon electromagnetic form factors provide a **"famous test"** for perturbative QCD. Brodsky and Farrar derived scaling rules for dominant helicity amplitudes which are expected to be valid at sufficiently high momentum transfers Q^2 [86]. Processes where the interactions among the quarks proceed via gluon or photon exchange, both of which are vector interactions, conserve the quark helicity in the limit when the quark masses or off-shell effects can be neglected. In contrast to the helicity conserving form factor F_1, the Pauli form factor F_2 involves a helicity flip between the initial and final nucleons. Hence it requires one helicity flip at the quark level, which is suppressed at large Q^2. Therefore, for collinear quarks, i.e. moving in a light-cone wave function state with orbital angular momentum projection $l_z = 0$ (along the direction of the fast moving hadron), the asymptotic prediction for F_2 leads to a $1/Q^6$ fall-off at high Q^2. For the proton ratio F_{2p}/F_{1p}, the polarization data up to 5.6 GeV^2 show no sign of a $1/Q^2$ behavior as predicted by pQCD. Instead, the data show that the ratio F_{2p}/F_{1p} falls less fast than $1/Q^2$ with increasing Q^2 as shown in Fig. 7.

Belitsky, Ji, and Yuan [67] investigated the assumption of quarks moving collinearly with the proton, underlying the pQCD prediction. They [67] showed that by including components in the nucleon light-cone wave function with quark orbital angular momentum projection $l_z = 1$, one obtains the behavior $F_2/F_1 \to \ln^2(Q^2/\Lambda^2)/Q^2$ at large Q^2, with Λ a

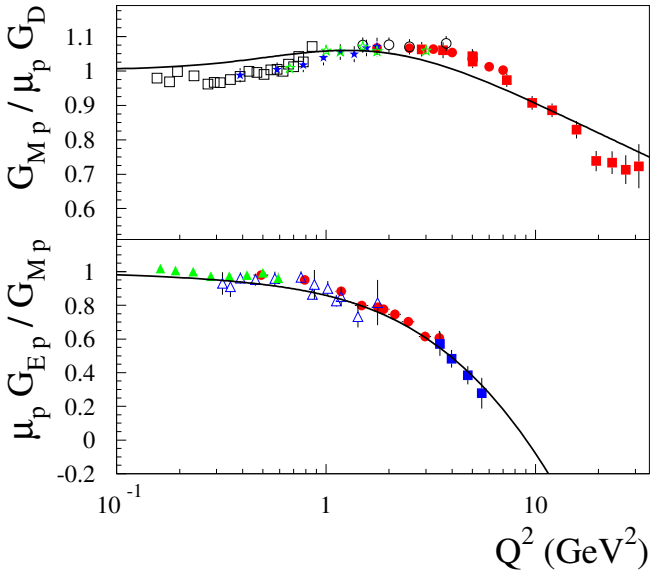

Figure 6: GPD calculation of the proton magnetic form factor relative to the dipole G_D (upper panel), and ratio of proton electric over magnetic form factors (lower panel), according to Ref. [58]. The dotted curves correspond to the Regge parameterization R1, with $\alpha' = 1.105$ GeV^{-2}. The solid curves are for the three parameter modified Regge parameterization R2 : $\alpha' = 1.105$ GeV^{-2}, $\eta^u = 1.713$ and $\eta^d = 0.566$. Data for G_{Mp} are from [60] (open squares), [61] (open circles), [62] (blue solid stars), [63] (green open stars), [10] (red solid circles), [64] (red solid squares), according to the recent re-analysis of Ref. [65]. Data for the ratio G_{Ep}/G_{Mp} are from [8] (blue open triangles), [5] (blue solid squares), [6] (red solid circles), and [66] (green solid triangles).

non-perturbative mass scale. Choosing Λ around 0.3 GeV, it was noticed in Ref. [67] that the data for F_{2p}/F_{1p} support such double-logarithmic enhancement, as can be seen in Fig. 7 (right panel). The arguments of Belitsky *et al.* [67] still rely on pQCD and it remains to be seen, if their model still applies at higher Q^2s of this proposal, as this prediction already agrees with the data in the few GeV^2 region.

Also in references [68, 69], it has been discussed that inclusion of quark orbital angular momentum yields a ratio F_{2p}/F_{1p} which drops less fast than $1/Q^2$ with increasing Q^2.

Lattice QCD calculations of nucleon structure quantities have matured considerably in the recent past. They provide quantities such as the nucleon electromagnetic form factors from the underlying theory of QCD. At present there is no systematic framework for extrapolating lattice QCD results for nucleon form factors at values of Q^2 larger than about 0.3 GeV^2. The development of such a framework remains a challenge for future work. Even when lattice results become available for m_π values below 300 MeV, at larger Q^2, one is faced with the problem of performing a chiral extrapolation (in the small scale m_π) in the presence of a large scale Q^2. A first attempt in this direction has been performed by Matevosyan *et al.* [70],

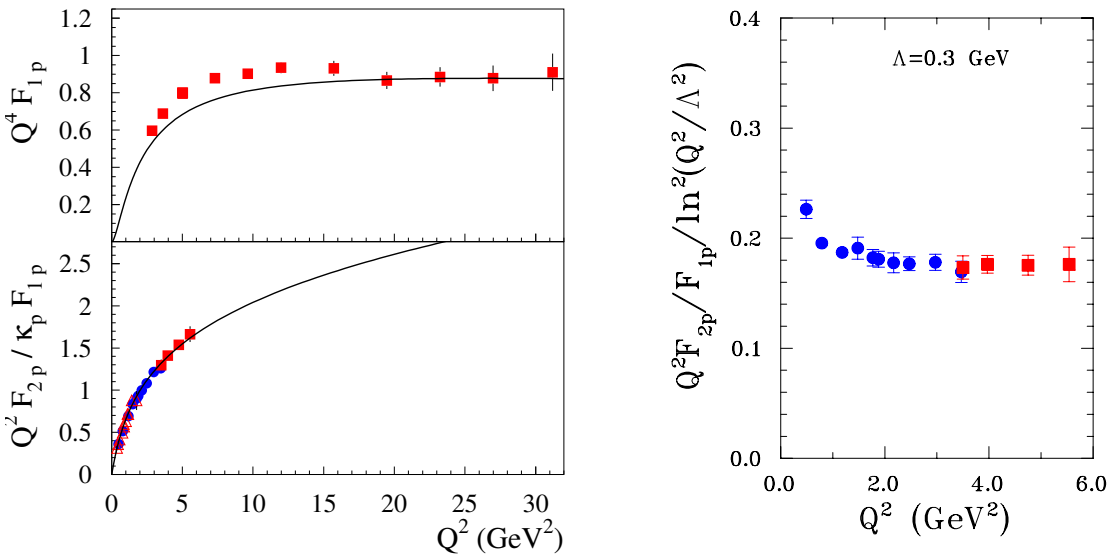

Figure 7: Test of the scaling behavior of the proton form factors. Upper left panel : proton Dirac form factor multiplied by Q^4. Lower left panel : ratio of Pauli to Dirac proton form factors multiplied by Q^2. Right panel : test of the modified scaling prediction for F_{2p}/F_{1p} of [67]. The data for F_{1p} are from [64] (solid squares). Data for the ratio F_{2p}/F_{1p} on both panels are from [6] (blue solid circles), [8] (red open triangles), and [5] (red solid squares). The curves on the left panels represent the calculation based on the three parameter modified Regge GPD parametrization of [58].

within the context of a light-front cloudy bag model (LFCBM). Fig. 4 shows predictions from Ref. [70] of the ratio G_{Ep}/G_{Mp} as a function of Q^2 up to 40 GeV^2.

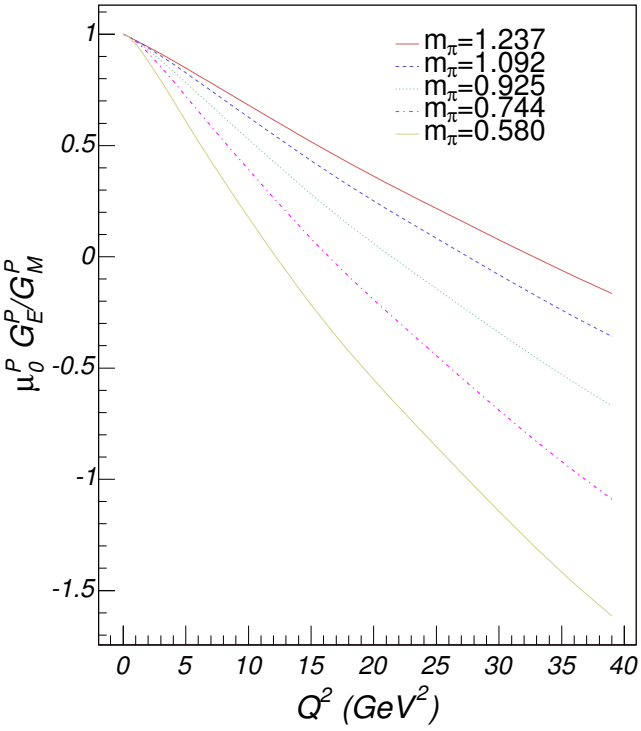

at

Figure 8: LFCBM calculations of Matevosyan *et al.* [70] (Fig. 13 in this reference), using parameters obtained by reproducing lattice results for the ratio G_{Ep}/G_{Mp}, at lattice spacing a=0.26 GeV^{-1}.

5 Evolution of the Polarization Transfer Experiments

5.1 The Method

In the one-photon exchange approximation the scattering of longitudinally polarized electrons from unpolarized hydrogen results in transfer of polarization to the recoil proton with two components, P_t perpendicular to, and P_ℓ parallel to the proton momentum in the scattering plane [71, 72]:

$$I_0 P_t = -2\sqrt{\tau\,(1+\tau)}\,G_E G_M \tan\frac{\theta_e}{2} \tag{6}$$

$$I_0 P_\ell = \frac{1}{m_p}\,(E_e + E'_e)\,\sqrt{\tau\,(1+\tau)}\,G_M^2 \tan^2\frac{\theta_e}{2}, \tag{7}$$

where $\tau = Q^2/4m_p^2$; E_e, E'_e, and θ_e are the initial and final electron energy and scattering angle, and $I_0 \sim G_E^2 + \frac{\tau}{\epsilon}G_M^2$. Measuring simultaneously these two components and taking their ratio gives the ratio of the form factors:

$$\frac{G_E}{G_M} = -\frac{P_t}{P_\ell}\frac{(E_e + E'_e)}{2m_p}\tan\frac{\theta_e}{2} \tag{8}$$

Using the polarization technique, the form factor ratio G_E/G_M at a given Q^2 can be obtained without measuring the absolute cross sections and without change of beam energy or detector angle, thus eliminating important sources of systematic uncertainties. Radiative corrections have been shown to be very small for polarization observables [4]. Note that the analyzing power of the polarimeter and the beam polarization that appear as a coefficient to P_t and P_ℓ, cancels out in Eq. 8, and their knowledge is not needed. However the efficiency of the experiment requires that these quantities must be maximized.

5.2 Experiments with 6 GeV accelerator

The first recoil polarization experiment (E93-027) [56, 6] at JLab used the two High Resolution Spectrometers in Hall A. The solid angle of the spectrometers is 6 *msr* and the momentum resolution 10^{-4}. A polarimeter placed in the focal plane of the proton arm measured the polarization components, P_t^{spec} and P_n^{spec}, of the proton perpendicular to its momentum. The polarization components at the target, P_t and P_ℓ, that enter in Eq. 8 were obtained from the measured P_t^{spec} and P_n^{spec}, using spin transport model of the spectrometer.

The acceptances of the two spectrometers approximately matched up to Q^2 values of 2.5 (GeV/c)^2. The electron to proton solid angle ratio, Ω_e/Ω_p, increases with Q^2 for a fixed beam energy. For the two highest Q^2 points at 3.0 and 3.5 (GeV/c)^2, the electron arm spectrometer was limiting the overall acceptance. That is why for the second GEP experiment (E99-007) [5], the electron spectrometer was replaced by a lead-glass calorimeter

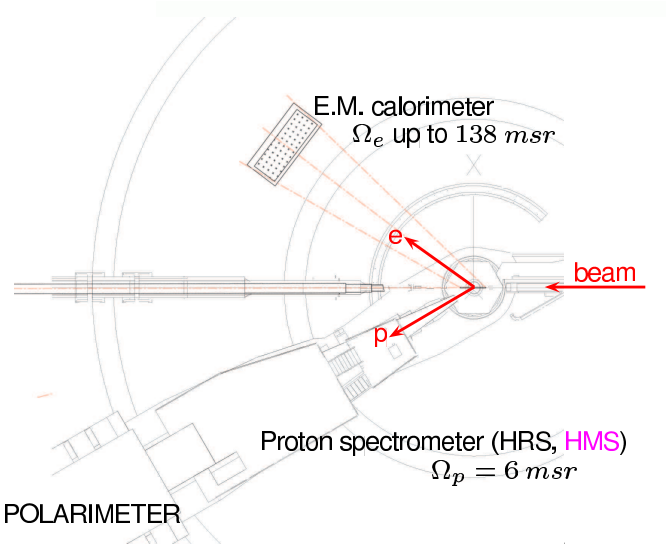

Figure 9: One High Resolution Spectrometer and one calorimeter set-up of GEP(2) in Hall A; similar set-up for the GEP(3) in Hall C.

of frontal area $1.3\,m \times 2.5\,m$ (Fig. 9). The distance to the target varied between $9 - 17\,m$ to achieve full solid angle matching and therefore maximize the number of events collected.

A similar solution was chosen for the forthcoming GEP(3) experiment (E04-108)[73]. It will use the HMS spectrometer (6.8 msr) in Hall C and the specially build lead-glass calorimeter, BigCal, with 1744 lead-glass blocks of $4 \times 4\,cm$ frontal area. This calorimeter provides much better electron angle resolution and can be placed very close to the target. Another improvement is the new Focal Plane Polarimeter (FPP) with two analyzers, that is expected to increase the overall Figure-Of-Merit (FOM) by about $20 - 30\%$. The highest Q^2 should be 9 $(GeV/c)^2$, with a 6 GeV beam, as proposed and approved; however, the exact value of Q^2 will be determined by the available beam energy at the time of the experiment.

5.3 Challenges of high Q^2 measurements

Form factor measurements above 9 $(GeV/c)^2$ can be done only with the 12 GeV accelerator. Doubling of the energy, however, is not the only condition for high Q^2 measurements.

The elastic ep cross-section, $d\sigma_{el}/d\Omega_{Lab}$ drops rapidly as $\sim E^2/Q^{12}$, where the main contribution comes from the form-factor part, $\sim 1/Q^8$, while the Mott cross-section is proportional to E^2/Q^4.

The analyzing power, A_y, of the reaction used to measure the proton spin falls as $1/p_p \sim 1/Q^2$ [74, 75], where p_p is the proton momentum in the lab frame. This is illustrated at Fig. 10 for the first two GEP experiments [6, 5]. In the GEP(1) experiment carbon was used as an analyzer, while in GEP(2) it was replaced by CH_2. After the proton rescattering the secondary charged particle is not identified. To demonstrate the $1/p_p$ dependence, the analyzing power, A_y, measured in these experiments, is multiplied by the proton momentum

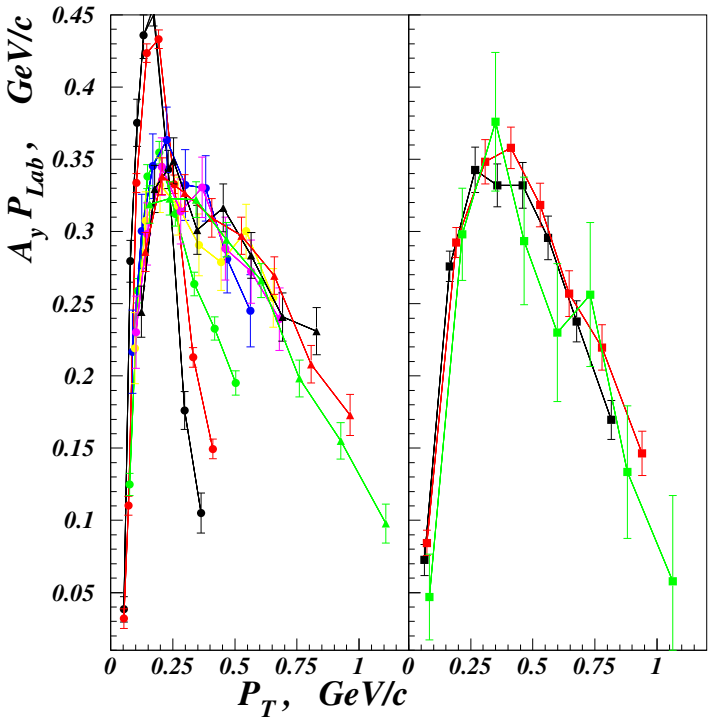

Figure 10: Analyzing power times proton momentum, $A_y P_{Lab}$, versus secondary particle transverse momentum, P_T. Left, for $p + C \to 1charged + X$ for different proton momenta: black, red, green, blue, yellow, magenta circles – 0.76, 0.99, 1.27, 1.46, 1.65, 1.71 GeV/c; black, read, green triangles – 2.07, 2.36, 2.64 GeV/c. Right, for $p + CH_2 \to 1charged + X$ for different proton momenta: black, red, green – 2.92, 3.37, 3.81 GeV/c.

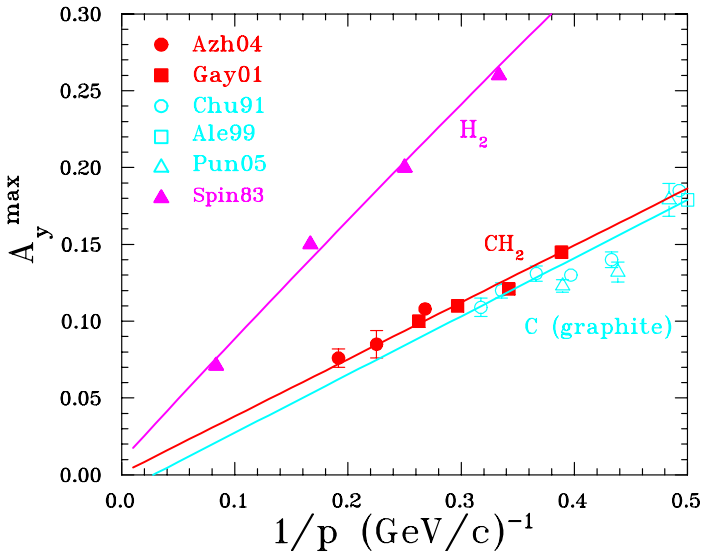

Figure 11: Maximal value of analyzing power, A_y^max, for the $p+C/CH_2 \to 1charged+X$ reactions (blue/red) from [74, 8, 78, 79, 6], and for the elastic pp reaction (magenta) [76] versus the inverse of the proton lab momentum

and plotted versus the transferred momentum $p_T = p_p\theta_{fpp}$. Here θ_{fpp} is the polar angle between the incident proton and the secondary charged particle registered in the FPP. One can see that starting at a proton momentum of about 1.5 GeV/c, the product p_pA_y exhibits similar behavior as a function of p_T. Such a scaling was found experimentally to be valid up to a proton momentum of 5.3 GeV/c [74] at the Dubna (JINR, Russia) accelerator. As a result, the effective analyzing power $A_y^{eff} = \int A_y dp_T$ is proportional to $1/p_p$. Here it is assumed that the polarimeter allows to register secondary particles with 100% geometrical efficiency up to values of p_T for which A_y vanishes.

At Fig. 11 we compare the maximal value of the analyzing power, A_y^{max}, for C and CH_2 including also the Dubna and other data. On the same figure the A_y^{max} value for the elastic pp reaction [76] is plotted. It exhibits similar $\sim 1/p_p$ behavior, but the values are about twice as large as compared to the $p + C(CH_2) \to 1charged + X$ reactions.

The overall experimental Figure-of-Merit, FOM is proportional to the number of elastic protons N_p and to the polarimeter Figure-of-Merit, FOM_{pol}. The latter in turn is proportional to the effective analyzing power squared, assuming constant polarimeter efficiency. Therefore, one can estimate $FOM \sim N_pFOM_{pol} \sim \sigma_{el}(A_y^{eff})^2 \sim E^2/Q^{16}$. For example, because of the rapid fall with Q^2, the FOM of a 14 (GeV/c)^2 measurement using the 11 GeV beam, is only 1/15 of the FOM of the highest Q^2 GEP(3) measurement at 8.5 (GeV/c)^2 with 5.7 GeV beam energy. Therefore, in order to get similar statistical errors at high Q^2, without using excessive beam time, one needs detectors with acceptances an order of magnitude larger than the one of the "classical" experimental set-up (Fig. 9).

Using a "classical" set-up at high Q^2 require new proton spectrometer since the proton momentum is proportional to Q^2 [80].

In high Q^2 measurements of G_{Ep}/G_{Mp} special attention should be paid to the accuracy of

the precession angle **in the non-dispersive plane of the spectrometer** which increases as $\gamma_p \sim Q^2$. Let us consider a simple magnet that bends proton trajectories at an angle of $\Delta\theta$ in a plane perpendicular to the reaction plane. In this plane the proton has only one spin component, the longitudinal one, P_ℓ [1]. After the magnet, it is rotated by a precession angle of $\chi_\theta = \gamma_p(\mu_p - 1)\Delta\theta$, where μ_p is the proton gyromagnetic ratio. Because of the large proton gamma factor, γ_p, even small bend angles are enough to rotate the P_ℓ component to about the optimum 90° for measurement in the polarimeter. At the same time, the precession in the reaction plane $\chi_\phi = \gamma_p(\mu_p - 1)\Delta\phi$, where $\Delta\phi$ is the deflection in the non-dispersive plane (due to fringe fields), results in a mixing of the P_t and P_ℓ components. Since their ratio, P_t/P_ℓ, is directly proportional the form factor ratio, such mixing is a source of systematic uncertainty.

To a good approximation [6, 77] the ratio of the polarization components at the target P_t/P_ℓ is related to the the measured ratio P_t^{spec}/P_ℓ^{spec} by:

$$\frac{P_t}{P_\ell} = \frac{P_t^{spec}}{P_n^{spec}} \sin\chi_\theta + \gamma_p(\mu_p - 1)\Delta\phi, \tag{9}$$

where the two terms represent the dispersive and non-dispersive precession. These terms appear in the result for the form factor ratio when substituting Eq. 9 in Eq. 8:

$$\mu_p \frac{G_E}{G_M} = -\mu_p \frac{E_e + E_e'}{2m_p} \tan\frac{\theta_e}{2} \left(\frac{P_t^{spec}}{P_n^{spec}} \sin\chi_\theta + \gamma_p(\mu_p - 1)\Delta\phi \right) \tag{10}$$

At high Q^2 the combined factor in front of $\Delta\phi$ becomes big, for example about 100 at $Q^2 = 14$ (GeV/c)^2. That is why the systematic uncertainty from the non-dispersive precession is about 100 times bigger than the uncertainty of the non-dispersive deflection angle $\Delta\phi$. For example 1 *mrad* error in the angle corresponds to 0.1 absolute error for the form factor ratio. Therefore, controlling the mean deflection angle in the reaction plane to a fraction of a *mrad* is mandatory for high Q^2 measurements.

[1] the normal component P_n is negligible since it is zero in Born approximation

6 Proposed experimental setup

The experiment will be performed in Hall A. The electron beam will pass through a 40 cm long LH2 target in the existing scattering chamber. The electron will be detected in the recently-built, highly segmented electromagnetic calorimeter BigCal. We propose to built a large acceptance proton arm, which trades the high resolution of HRS-HMS-SHMS for a large acceptance and moderate momentum resolution. In the following sections the details of such a setup and its operation at the required luminosity are presented. The layout of the

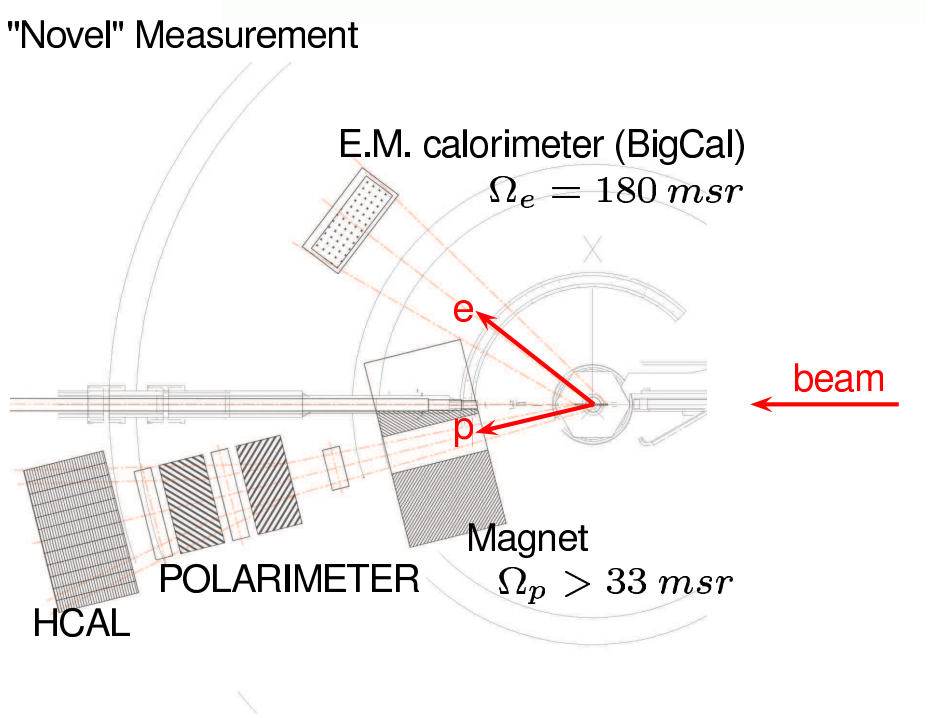

Figure 12: The proposed large acceptance setup. Proton arm: 48D48 magnet, double polarimeter with three blocks of fast tracking chambers, and a hadron calorimeter. Electron arm: 1744 channel electromagnetic calorimeter.

proposed experimental set-up is shown in Fig. 6.

An existing simple (non-superconducting) magnet, type 48D48, is placed close to the target providing a solid angle $> 33\ msr$. The magnet can view a target of 40 cm length. The magnet is followed by a polarimeter and a hadron calorimeter, HCAL. The polarimeter consists of two CH_2 analyzers with tracking chambers on both sides of each analyzer. The hadron calorimeter, with an energy resolution of about 30% for high energy protons, has two important functions. First, the calorimeter provides a trigger with a high threshold of 4 GeV to reduce the DAQ rate. Second, it provides both coordinates of the hadron shower with an accuracy of 1.5 cm, greatly facilitating the tracking analysis in the presence of a very high hit multiplicity.

The price one has to pay for having a large acceptance are the high background rates especially at the front chambers which are in direct view of the target. However, the invention

by F. Sauli of the Gas Electron Multiplier (GEM) [81] has stimulated amazing progress in tracking technology during the last decade, and makes it possible to handle rates orders of magnitude higher than needed for this experiment, as discussed later in this section. We propose to use GEM based trackers described in the articles [81, 82]. The GEM is based on gas avalanche multiplication within small holes, etched or drilled in a metalized Kapton foil. Such a technology gives a true two-dimensional localization of the radiation. The avalanche is confined in the hole, free of photon-mediated secondary effects, resulting in very fast (few ns rise time) signals. All these properties result in very high rate capabilities of up to 100 MHz per cm^2.

6.1 CEBAF polarized beam

We assume a 75 μA beam with 85% polarization. Such a polarization has already been obtained in many JLab experiments. The beam polarization defines the magnitude of the measured asymmetries but the polarization transfer method doesn't require its knowledge to obtain the form factor ratio. The beam polarization will be measured with the Hall A Møller/Compton polarimeters to make sure that it is maintained at maximum level.

6.2 Target

A 40 cm liquid hydrogen target will be used. In addition a thin carbon target, as well a target consisting of 11 thin carbon foils with 4 cm spacing will be used for optical and spin transport studies in the proton arm as described in Section 8.

6.3 Rate estimates

To estimate the background rates we have used a simulation code written by P.Degtiarenko. This code has been used for many years at JLab to estimate experimental radiation budgets. To the standard GEANT-based model of Hall A we have included the proposed set-up as described in Fig.13. The results of these simulations are summarized in Table 1. The rates are calculated for 40 cm liquid hydrogen target with two 5mil Al walls, and 75 μA current. Charged particles with momenta less than 1 GeV don't contribute to the rates because they are swept out by the the magnet (3 Tm field integral). For photons two thresholds have been calculated to illustrate the two different types of background discussed in Section 6.4.3. Soft photons can produce uncorrelated random hits in the three chambers of a tracker, while those of greater than 300 MeV producing charged particles produced in the first chamber can mimic an actual track through the three chambers. The gamma efficiency of the chambers is discussed further in Section 6.4.3.

6.4 Proton arm

The proton arm is the new element in the proposed experiment. It consists of a dipole magnet providing the horizontal main field, a tracking system and a hadron calorimeter for the trigger. The detailed geometry of the set-up in the reaction (horizontal) plane is shown at Fig.13. The magnet bends vertically at an angle of 6° for the central trajectory. Using a

particle and threshold	front chamber at 325 cm	first rear chamber at 457 cm	second rear chamber at 556 cm
γ, 100 KeV	80,000	6,700	1,800
γ, 300 MeV	140	12	5.5
e^- ,1 GeV	0.3	0.05	0.02
e^+ ,1 GeV	0.2	0.03	0.01
π^- ,1 GeV	8	1.2	0.54
π^+ ,1 GeV	14	2.1	0.95

Table 1: Estimated rates in kHz per cm^2 at different distances from the target for different particles integrated above the given thresholds; for 40 cm LH target and 75 μA

simple magnet without quadrupoles makes it easier to control the non-dispersive deflection as discussed in Section 7.2. The horizontal:vertical aspect ratio of the set-up is about 1:2.

6.4.1 Dipole magnet

The magnet of the proton arm is a type 48D48 dipole, four of which were used in fixed target experiments at AGS, and presently available together with the power supply. The magnet has a total weight of 100 tons. It consists of five iron slabs and two saddle type coils. Such segmentation will make it possible to assemble the magnet in Hall A by means of the available 20-ton overhead crane. The magnet has a 46 cm wide gap between 120×120 cm poles. When located at a distance of 150 cm from the target, it provides 35 msr solid angle at 14°. Installation of such a large magnet at the required angle close to the target interferes with the beam line and thus we plan to make an opening in the magnet iron for the beam line, as shown in Fig. 14. The effect of such a modification on the field in the gap is relatively small as it was confirmed by a full calculation with TOSCA code. With a 1 Tesla field in the gap, there is only 7 Gauss in the opening for the beam line. This field will be further reduced at the beam center by means of a thin μ-metal shield. Outside the magnet iron, field clamps, and beam-line shielding will be used to insure a low field level in the beam line.

In Hall A the magnet will be installed on rails similarly to the ones used in the GEN (E02-013) experiment for the 80-ton neutron detector. After assembly the magnet will be manually moved to the final position. Then a section of the beam line vacuum pipe will be inserted through the right coil and connected with the rest of the vacuum pipe.

6.4.2 Polarimeter

The polarimeter measures the proton polarization in a plane perpendicular to the trajectory using the azimuthal asymmetries of the proton-analyzer scattering (see Section 7.2). We propose a polarimeter with two 50 cm CH_2 analyzers, very similar in geometry to the one constructed for the GEP(3) experiment. The main difference is that the original drift chambers will be replaced by high rate tracking chambers, described in the next subsection 6.4.3. The feasibility of using such polarimeter has been experimentally supported by calibration measurements at the Dubna accelerator [74]. This double polarimeter will be used as two independent polarimeters in series.

As seen from Fig.10, the analyzing power vanishes for P_T values above 1.2 GeV/c. For the momentum range of $7.5-9.5$ GeV/c of the proposed high Q^2 measurements, it corresponds to polar scattering angles θ of $7.2-9.2^\circ$. The dimensions of the polarimeter were chosen in such a way as to allow for secondary scattering with full geometrical efficiency up to 10° from both analyzers (Fig.13).

The analyzing power has a maximum at $P_T \approx 0.4\ GeV/c$ (Fig. 10), corresponding to polar angles of $40-50$ $mrad$, and then drops rapidly at smaller angles. Thus, for the polarimetry it is sufficient to have an angular resolution of about 2 $mrad$. Multiple scattering angle uncertainties in the analyzers will be $1.5-2$ $mrad$ depending on the proton momentum.

The hadron calorimeter requires the secondary particle to be above the threshold of 4 GeV (Section 6.6), which means it is most likely a proton (the elastic cross-section is $\sim 25\%$ of the total one). In contrast, in the GEP experiments there was no constraint on the secondary particle except that it be charged. This is the case for all the C and CH_2 measurements presented at Figure 11, for which the analyzing power is about half the value for the elastic pp reaction. That is why we expect that by applying a threshold on the secondary particle the analyzing power, A_y, will increase. At the same time the polarimeter efficiency, ε will decrease, but since the polarimeter FOM is proportional to the εA_y^2, the expectation is again in favor of increasing FOM. However, this needs to be confirmed experimentally before the experiment, as explained in Section 8. For the purposes of the error estimations we assume a constant polarimeter efficiency of 25% for each analyzer, while the analyzing power is extrapolated from Figure 11.

6.4.3 Tracking chambers

We propose to built three trackers (GEM, TGEM1, and TGEM2 at Fig. 13), each consisting of three GEM chambers. Each chamber gives three coordinates (x,u,v) by means of three layers of readout strips on which charge from the chambers is induced. The front tracker will be used both as part of the spectrometer, and of the polarimeter. The rear trackers are needed only for polarimetry. The background rates (Table 1) at the front chambers are about 10 times bigger than at the rear chambers, and dominated by photons. All this implies different requirements, and therefore different solutions for the type of the front and rear chambers.

For the front chambers we propose to use the standard thin GEM technology [81]. The typical foil thickness and hole diameter are $50-70$ μm and the pitch is 100 μm. The amount of material can be as low as 50 mg/cm^2. For such a material we estimate about 10^{-3} efficiency for gamma detection. From Table 1 we obtain about 100 kHz/cm^2 (80 kHz/cm^2 photons and 20 kHz/cm^2 pions) rates on the front chamber, which is three orders of magnitude less that the GEM technology limit.

Figure 15 shows one of the 20 GEM detectors [83] which have been operational for several years at the COMPASS experiment at CERN. It has three 31×31 cm^2 GEM foils inside the gas volume, that give triple amplification and allow for stable operation at high gains.

In the proposed setup the front GEM tracker should cover an area of 40×75 cm. Due to the limitations of the thin GEM technology, the front chambers will consist of two GEM 40×40 cm^2 sections with an overlapping region in the middle.

The high rates will also produce random hits in the chambers. Using a standard 100 ns integration time, the probability of random hits on the front chambers will be 1% per cm^2. Since the photon hits on the three GEM chambers are not correlated they can be eliminated. A residual of 20% corresponds to random tracks, mostly from pions that appear with a probability of 0.2% per cm^2. Section 7 explains how to deal with these tracks.

We require a 0.2 $mrad$ angular resolution of the front tracker, a value similar to the contribution of the multiple scattering in the air between the target and the tracker. This can be achieved with a distance of about 50 cm between the side GEM chambers, as the thin GEM chambers have a superior coordinate resolution of about 70 μm. Magnet simulation with the SNAKE code including also the multiple scattering in the air between the target and the tracker, shows that this will correspond to a momentum resolution of the spectrometer of 0.5% at a bending angle of 6°, and to an in-plane and out-of-plane angular resolution of 0.3 $mrad$.

Since we require only 2 $mrad$ angular resolution for the rear trackers (Section 6.4.2), we propose to use there thick GEMs. Such technology was recently developed [82] as a much cheaper alternative to the standard GEM when the required coordinate resolution is of the order of sub-millimeters. Thick GEMs can be build with bigger sizes. Such detectors have very stable performance, and the same high rate capabilities. Typically all the GEM dimensions (foil thickness, hole diameter and pitch) are about 10 times bigger than in the thin GEM. A resolution of 0.3 mm has been achieved. This means the distance between the side chambers in the tracker should be about 20 cm. The rear blocks should cover areas of 100×200 cm.

The photon efficiency of the thick GEM chambers is expected to be 10 times higher, $\sim$ 1%. Therefore, although the photon rates are $\sim$ 10 times smaller (Table 1) we expect 70 kHz/cm^2 on these chambers, which rate however is reduced to a few kHz/cm^2 after eliminating the random hits.

6.4.4 Hadron calorimeter

The hadron calorimeter [84] consists of an array of 11×22 modules, each $15 \times 15 \times 100$ cm^3. These modules were built in JINR, Dubna (Russia) and are now used in the COMPASS experiment at CERN. One module consists of 40 iron/scintillator plates of 20/5 mm thickness, a wave-length shifter, a PMT, and a base. (Fig.16).

The energy resolution of a prototype array of 5×5 modules was measured [84] to be $(59.4 \pm 2.9)/\sqrt{E} + (7.6 \pm 0.4)\%$. The coordinate resolution in both direction was found to be 14 ± 2 mm.

6.5 Electron arm

The 1744 channel lead-glass electromagnetic calorimeter BigCal, constructed for the GEP(3) experiment, will be used to register the electrons. The calorimeter was tested in the Testlab (Fig.17) and as of June 2007 it is being prepared for transportation to Hall C for the forthcoming experiments starting this fall.

Glass blocks, contributed by IHEP, Protvino, of sizes 38x38x450 mm^3 form an array of

32x32 blocks. On the top of it, an array of 30x24 blocks of sizes 40x40x400 mm^3 that came from the RCS experiment, is stacked. In both the Protvino and RCS parts the same PMTs are used ("FEU-84") optically coupled to the glass using "cookies" with a thickness of about 5 mm.

The individual signals from each channel are amplified in front-end modules and sent to Fastbus ADC modules LeCroy 1881. Analog sums of each 8 channels are sent to Fastbus TDCs LeCroy 1877 via discriminators. Analog sums of 64 channels are fed into discriminators that form a logical OR of all the channels used as an electron arm trigger. The pedestal widths (sigma) are about 2 MeV for the individual channels, and 15 MeV for the sum of 64, which together with the detector resolution, defines the precision of the trigger threshold.

By means of detailed GEANT simulations of the calorimeter, the coordinate resolution was estimated to be $5-10$ mm depending on the electron angle and energy. The calorimeter will be placed at 3.5 m which corresponds to an angular resolution of ~ 2 $mrad$. Based on the results of the RCS experiment [88], we expect less than $\sim 5\%/\sqrt{E}$ energy resolution. For the minimum electron energy of 2.5 GeV (at Q^2=16 GeV^2) the resolution will be $\sim 3.2\%$ which, when combined with the threshold precision, allows setting calorimeter threshold at about 2.2 GeV.

Course calibration using cosmic muon tracks has been done at a level of 10%. (Fig.18). In the forthcoming Hall C experiments the calorimeter will be calibrated precisely using elastic ep scattering and measuring the proton momentum in the HMS. For the proposed experiment, after identifying the elastic electron (see Section 7) its energy will be calculated from its angle. The angular resolution of 2 $mrad$ corresponds to $\sim 0.1\%$ electron energy resolution – more than sufficient for the calorimeter calibration.

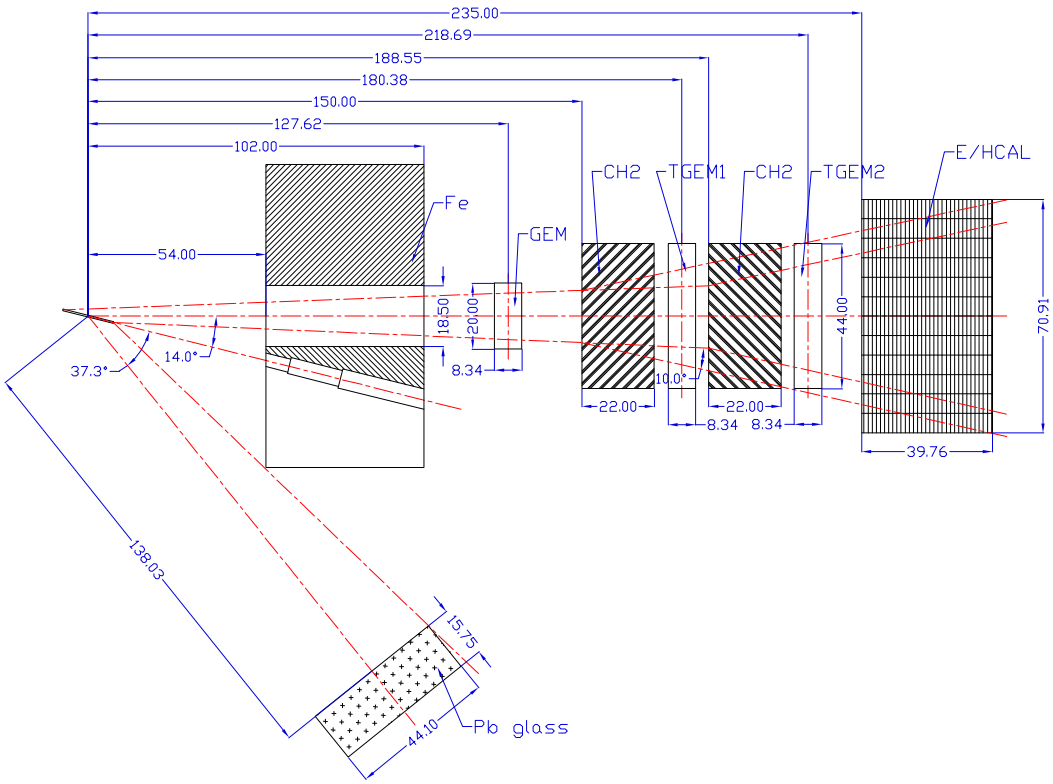

Figure 13: Detailed geometry of the proposed set-up in the reaction plane for the high Q^2 measurement. All dimensions are in inches.

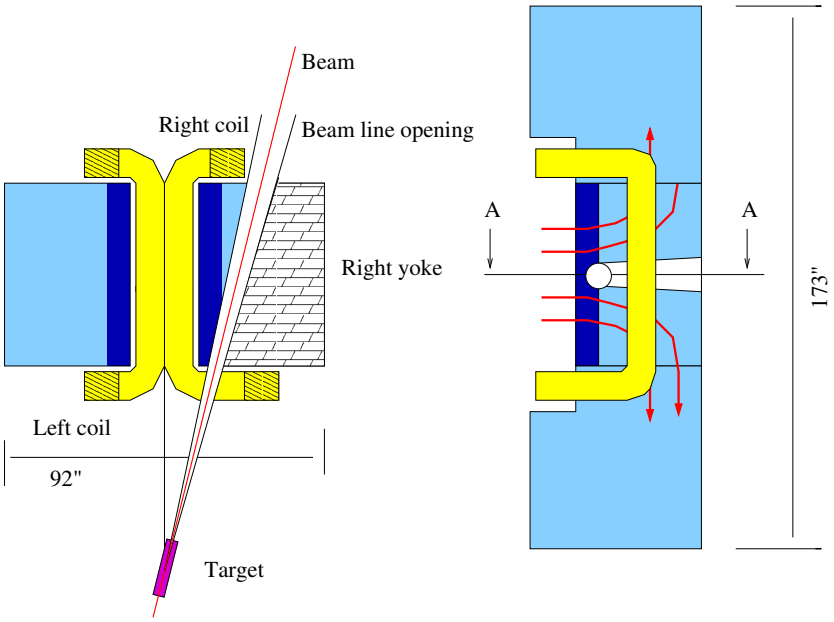

Figure 14: A sectional top view (left) and a front view (right) of the magnet. The right coil is modified to allow for the beam line passage. The beam line has a conical pipe (±40 mrad). The field lines (red curves in the right picture) show why the opening has just a little effect on the magnet properties.

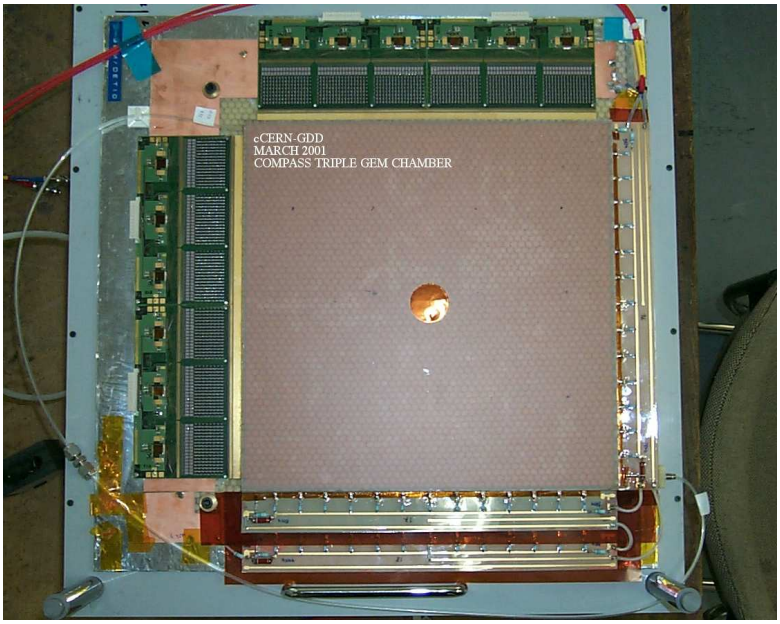

Figure 15: Triple GEM detector [83] operated in the COMPASS experiment at $2.5 MHz/cm^2$ rates. The hole inside is for the beam and will not be required for our application.

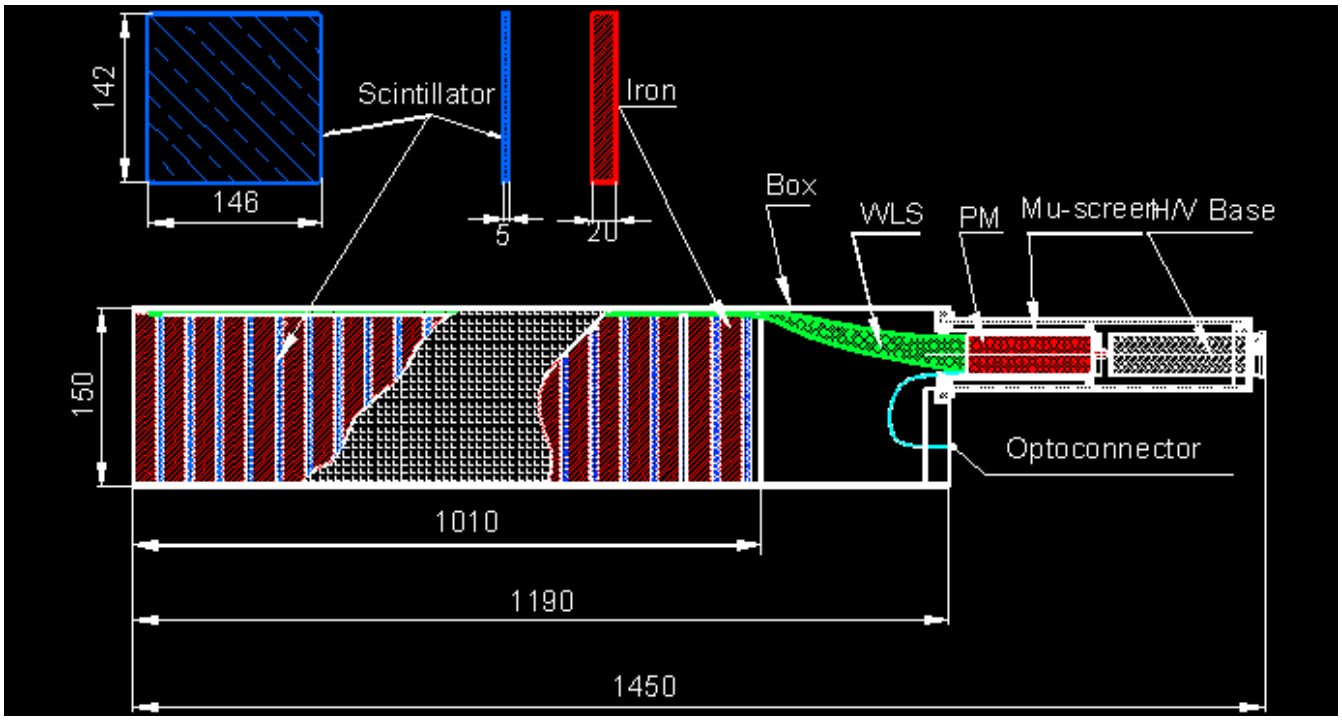

Figure 16: One module of the hadron calorimeter [84]. All dimensions are in *mm*.

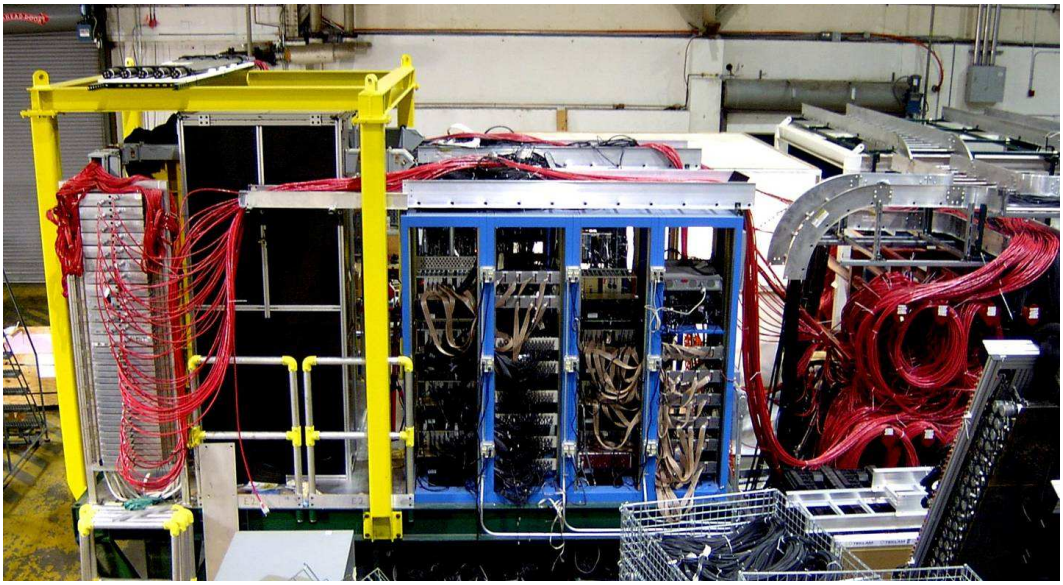

Figure 17: BigCal in Testlab, January 2007. 1744 lead-glass blocks, photo-tubes, and bases within the black box (left side with yellow frame), front-end electronics (blue racks), connected with HV (red) and signal cables (black) to the electronics platform (at the far right end).

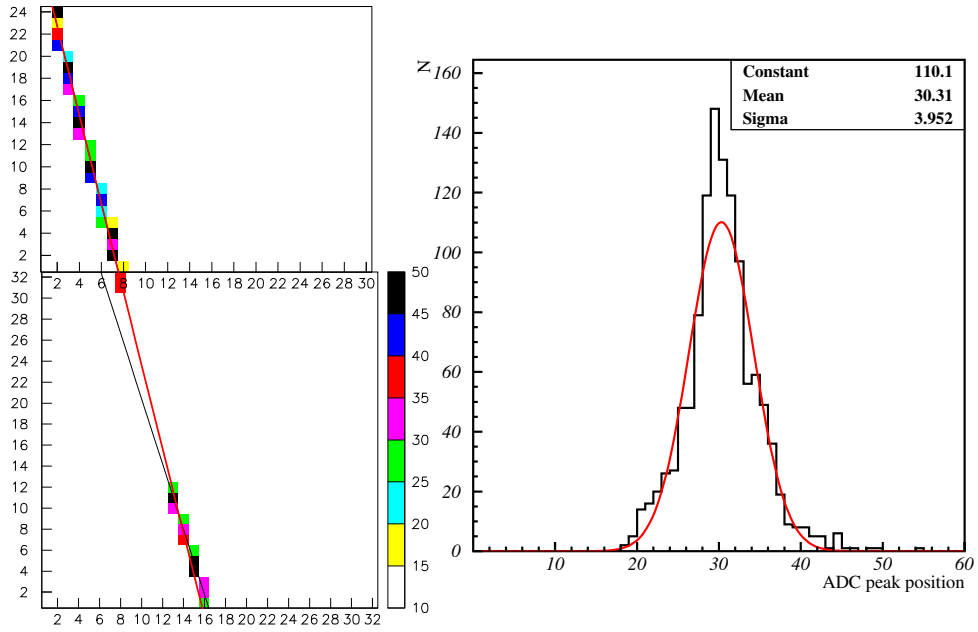

Figure 18: Left: one muon track through Protvino (bottom) and RCS (top) parts; colors represent ADC channel values, missing part of the track is in the region without HV, supposed to be supplied only in the hall. Right: ADC peak positions (in channels) after rough calibration with cosmic.

6.6 Trigger

There are several requirements to the trigger of the proposed experiment. First, it should be efficient for the events of elastic electron scattering. Second, the frequency of the trigger should not exceed capability of the DAQ system. Electron arm trigger will be used as a first level DAQ trigger (L1). A coincidence between trigger signals of the two arms within a 50 ns time interval will be used as a second level DAQ trigger (L2). A CPU dead time associated with the Fast Clear rate expected to be of 6-8%.

The rate in the electromagnetic calorimeter at 5.75 GeV beam energy was measured (E99-114 [88]) to be about 11 kHz with 20 μA on 15 cm LH2 target at a threshold of 50% of the elastic peak value. The RCS calorimeter had face area of 0.88×1.28 m^2 and was located at a distance 8.1 m and an angle of 41° relatively to the beam. The rate as a function of the threshold measured in the experiment is shown in Fig. 19 from Ref. [89]. In the kinematics of

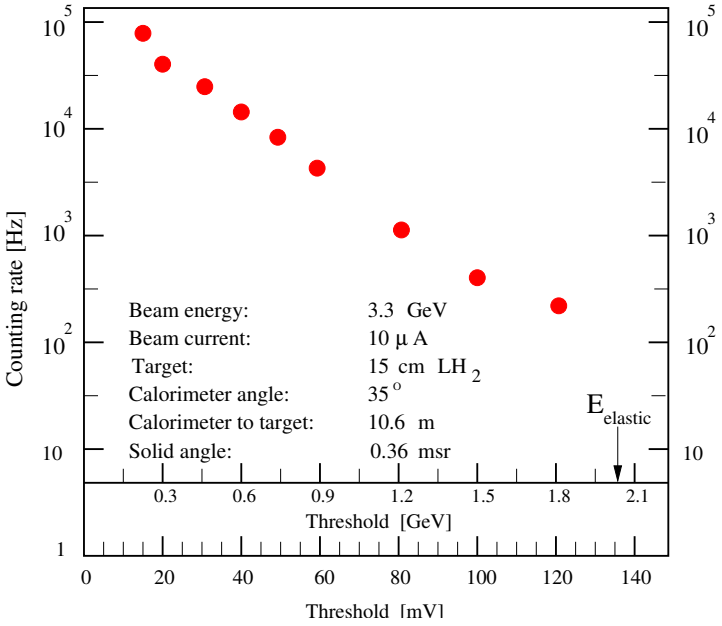

Figure 19: Typical dependence of the counting rate in the electromagnetic calorimeter vs the threshold level.

the RCS experiment we observed that the counting rate, f, had an exponential dependence on the threshold, E_{thr}, normalized to E_{max}, the maximum energy of an elastically scattered electron for a given scattering angle. This could be expressed as:

$$f = A \times \exp(-B \times E_{thr}/E_{max}),$$

where A is an angle-dependent coefficient, and B is a constant $\approx 9 \pm 1$. We also performed this type measurement for a higher beam energy of 5.75 GeV and used these for the rate estimate shown below. The angular variation of A, after normalization to a fixed luminosity and a calorimeter solid angle, is less than a factor of 2 for the RCS kinematics. The electron arm calorimeter in proposed experiment, BigCal, will cover solid angle of 215 msr at a central angle of 37.3°. The neutral and charged pions made the dominant contribution to the rate in

the calorimeters for electron beam energies above few GeV and a perpendicular momentum of about 0.5 GeV/c.

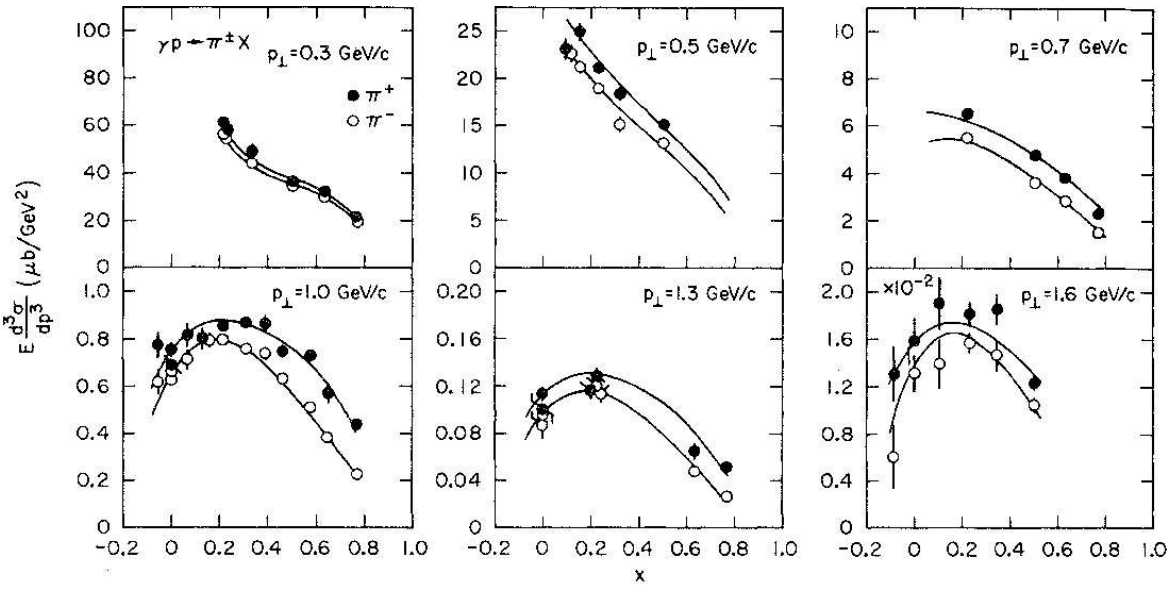

Figure 20: Inclusive cross section of pion photo production at large photon energy from Ref. [85].

For the calculations of the trigger rate in the electron arm of the proposed experiment (Table 2), the above RCS experimental results as well as the experimental data from SLAC at high photon energies of 9-18 GeV [85] (see Fig. 20) have been used. Because of the large

E_{thr}/E_{max}, %	50	75	85	90
Rate, kHz	1400	148	60	38

Table 2: Electron arm trigger rate as a function of the percentage of the threshold to the elastic energy.

angular acceptance of the calorimeter, the energy of the elastically scattered electron varies between 4.45 and 2.48 GeV. As a result, the optimum value of the threshold also should vary depending on the horizontal position of the blocks in the calorimeter. We plan to use a threshold of 85% of the elastic scattering energy (see the discussions in Section 6.5).

High rates of particles in the proton arm present the main challenge in this experiment. The dipole 48D48 sweeps out all charged particles with momenta below 1 GeV/c. The remaining rate is dominated by high energy pions. Because the protons of interest have a large energy of 7.5-9.5 GeV we can use a high threshold of 4 GeV for the trigger. At such threshold the expected rate calculated on the basis of SLAC data [85] is 1.5 MHz of $\pi^{\pm}$ mesons. In the hadron calorimeter the combined signal from four adjacent modules will be used to form a logical signal.

The trigger logic for the electron arm is shown at Fig. 21. Each numbered sum combines four groups of four lead-glass blocks. In total there are 91 numbered sums. They overlap,

as shown for example for sum 16. Similar arrangement will be made for the hadron arm. A total of 210 logical signals of this type from the proton arm and 91 signals from the electron arm will be used to form a second level trigger of DAQ. The coincidence scheme will take into account the angular correlation between the electron and the proton. The angular correlation is limited by the proton scattering cone in the material of CH_2 analyzer. Nevertheless the correlation allows to reduce the accidental rate by a factor of 10. A 50 ns coincidence time for 60 kHz from the electron arm and an effective 0.15 MHz from the proton arm results in accidental rate of 500 Hz, which should be acceptable for the DAQ.

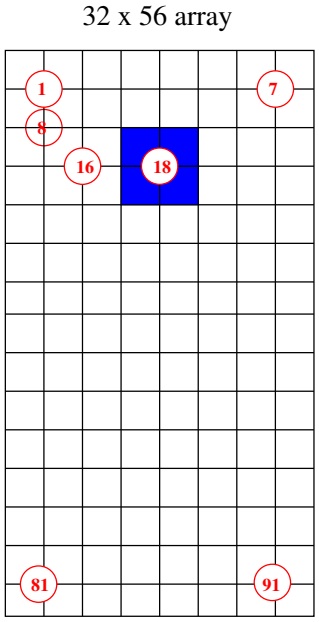

Figure 21: Trigger logic for the electron arm. The matrix of the lead-glass blocks has 32 vertical columns and 56 horizontal layers. Sums of the analog signals from each group of 4x4 blocks are sent to discriminators (for simplicity of the drawing only few sums are shown).

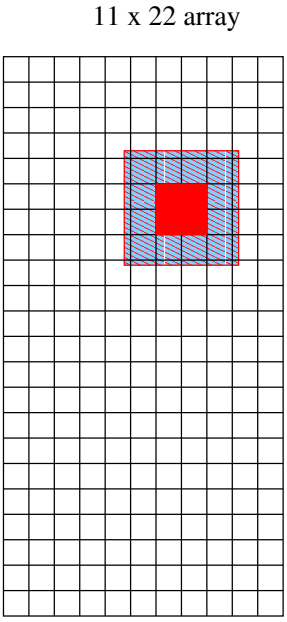

Figure 22: Trigger logic for the proton arm. The matrix of the blocks has 11 vertical columns and 22 horizontal layers. Sums of the analog signals from each group of 2x2 blocks are sent to discriminators. In the analysis larger area (4x4) blocks are used for the energy and hit coordinates determination.

7 Data analyzes

7.1 Tracking

Because of the high hit multiplicity in the trackers for the high Q^2 measurements, the track reconstruction procedure requires special explanation.

We start from the reconstructed electron hit on the calorimeter with a coordinate resolution of about 7 mm, positioned at a distance of 3.5 m from the 40 cm target.. Taking into account the size of the target, the corresponding elastic proton is expected in a region on the front tracker with a vertical width of 2 cm and a horizontal size of 13 cm. The horizontal size is defined mainly by the interaction point at the target. The vertical size reflects the uncertainty of the proton out-of-plane angle of about ± 3 $mrad$ (3σ), while the effect of the momentum variations is negligible. On such an area we expect (Section 6.4.3) 0.20 random photon hits and 0.06 (mostly pion) tracks through all the GEM chambers. As explained in Section 6.4.3 the soft ($0.1 \sim 300$ MeV) photon hits are not correlated and can be eliminated by a straight line requirement through the three chambers. For the remaining tracks the particle momentum is reconstructed with a 0.5% resolution. One can reconstruct also the in-plane angle with a 0.3 $mrad$ resolution, the in-plane coordinate of the interaction point (1 mm resolution for the proton and 2 mm for the electron side), and the electron in-plane angle with a resolution of 2.1 $mrad$. By correlating the kinematic information from the two arms, pion tracks will be rejected.

On the other hand, we have the proton position reconstructed at the hadron calorimeter with a resolution of 15 mm. This corresponds to an area on the last rear tracker of about 64 cm^2 where together with the proton track, we expect also a pion track in 1% of the cases (Section 6.4.3). One can reject such events, which will slightly (by 1%) reduce the track reconstruction efficiency, or one can save them by matching the tracks back to the middle and the first tracker, where only the proton tracks were kept.

As a result, we expect to identify the proton tracks at the front and at the last tracker. The two polarimeters work in series and we consider events when there was a scattering in the first or in the second analyzer. We extrapolate the tracks both from the front and from the last tracker to the middle one defining two spots of about 1 cm diameter (due to the multiple scattering in the analyzers and the angular resolution) one of which should contain the proton track. In such an area the probability of a random track is negligible.

A similar approach was successfully used for the reconstruction of the tracks in the BigBite chambers of the GEN experiment in Hall A. Figure 23 shows one event with the hits in the three BigBite drift chambers in front, and in the two sections of the electromagnetic calorimeter. The electron track is reconstructed by matching the crossing points of the three coordinates of each chamber with the calorimeter hits.

In conclusion, having three coordinates per chamber and three chambers in a row, as in the proposed experiment, helps greatly to reduce the noise and the soft photon hits. The remaining background of charged particles is suppressed by matching the tracking information with the electromagnetic and hadron calorimeter hits. Using the elastic kinematics to match the electron hits with the proton tracks is essential in this procedure.

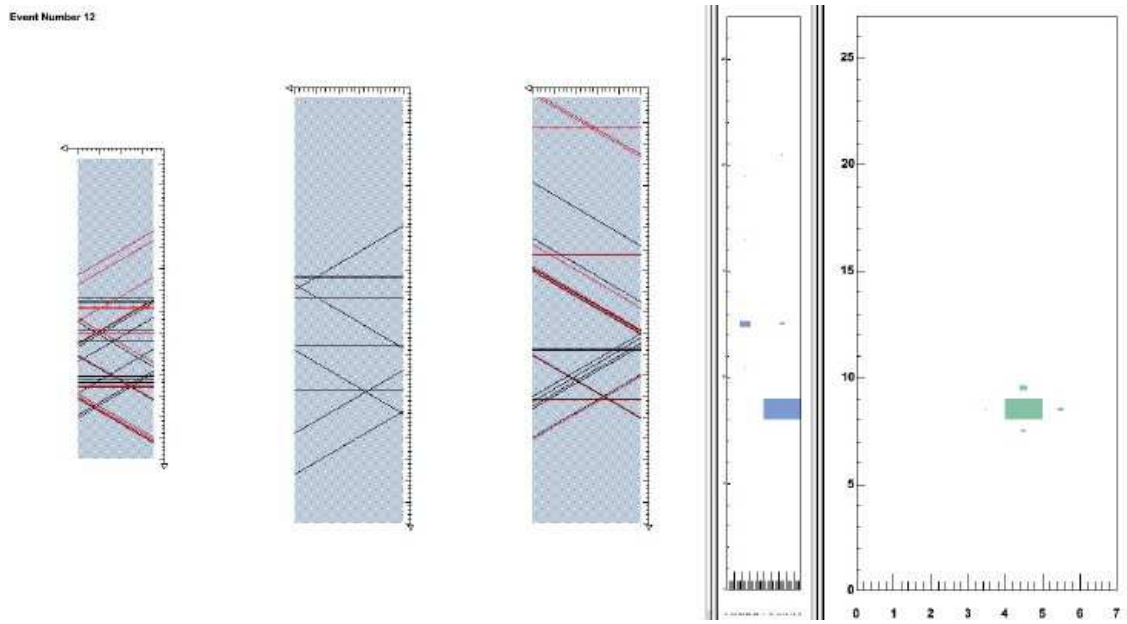

Figure 23: One event of the GEN experiment, with the BigBite arm detectors: three drift chambers and two sections of the calorimeter. The faces of the detectors are rotated to show the wires fired and the hits.

7.2 Polarimetry and spin transport

The probability of detecting a charged particle after the scattering in one of the analyzers, at a azimuthal angle , ϕ, and a polar angle, θ, is given by:

$$f^{\pm}(\theta,\phi) = \frac{\varepsilon(\theta,\phi)}{2\pi}\left(1 \pm P_e A_y(\theta)(P_t^{spec} sin\phi - P_n^{spec} cos\phi)\right) \ , \tag{11}$$

where $\pm$ denotes the sign of the beam helicity, P_e is the degree of the beam polarization, and $\varepsilon(\theta,\phi)$ is the detector efficiency. By means of a Fourier analysis of the the asymmetry:

$$A(\theta,\phi) = \frac{f^{+}(\theta,\phi) - f^{-}(\theta,\phi)}{f^{+}(\theta,\phi) + f^{-}(\theta,\phi)} = P_e A_y(\theta)(P_t^{spec} sin\phi - P_n^{spec} cos\phi) \tag{12}$$

one can determine the two polarization components P_t^{spec} and P_n^{spec} which, using the spin transport matrix, are related to the proton polarizations at the target, P_t and P_l. Note that the detector efficiency $\varepsilon(\theta,\phi)$ cancels out in the asymmetry and doesn't introduce false (instrumental) asymmetries.

The simple magnet used to rotate the longitudinal spin component, P_l so that it can be measured in the polarimeter, makes it easy to model the spin transport within the magnet. All the methods used in the GEP experiments are applicable here. In addition the view of the chambers from the target allows to directly relate the target and polarimeter coordinate systems. It is very important to note that the magnet deflection in the non-dispersive plane is very small and easily controlled. Simulations with SNAKE code show a sigma of the dispersive angle deflection of 0.6 *mrad*.

7.3 Background separation

The suppression of the random hits and tracks has been discussed before (Section 7.1). The spectrometer momentum resolution of 0.5% together with the angular resolution of the proton and electron arms of 0.3 $mrad$ and 2 $mrad$, respectively, helps to identify the elastic reaction and reject most of the background.

However, Bremsstrahlung in the target and subsequent $\gamma p \rightarrow \pi^0 p$ can mimic the ep elastic scattering because a photon from the π^0 decay will produce a similar signal in the electromagnetic calorimeter as the elastic electron. The two reactions have similar kinematics for the end point photon energies, because the pion mass (as is the electron mass) is negligible compared to the proton mass.

The π^0 background appeared in the GEP(2) experiment and was identified and rejected by correlating the HRS and calorimeter information. Here, we start with this experimentally obtained proton distribution of the background reaction then scale it for the kinematics of the proposed experiment and fold it according to the resolution of the proposed spectrometer.

According to [86] the cross-section of the $\gamma p \rightarrow \pi^0 p$ reaction falls as $1/s^7$. This was found to be in approximate agreement with the experiment [87] in the energy region of $4 - 5$ GeV (Fig.24). We use such an energy dependence for a backward center-of-mass angle of $\sim 135^\circ$ (for the high Q^2 measurement), to extrapolate the cross-section up to 11 GeV. Actually, it will give an upper limit of the cross-section. For low values of s and for backward angles the scaling condition $s, -u, -t \gg \Lambda^2_{QCD}$ is not fulfilled and the cross-section is enhanced because of u-diagram dominance. This is the case for the SLAC measurements where the u-invariant is about -1.2 GeV^2. For the proposed 11 GeV measurements $u \approx -5.3$ GeV^2 and the u-diagram contribution is much smaller. As a result the cross-section falls for energies between 5 and 11 GeV much faster than $1/s^7$. A similar effect was observed experimentally in real Compton scattering [88].

Using the above procedure we calculate the proton, π^0 and photon distributions and apply the elastic kinematical constraints. Fig.25, where the missing energy (E_{miss}, difference between the calorimeter energy and the one expected from the proton arm for elastic kinematics) distribution is plotted, illustrates that the π^0 background to be suppressed down to a value of 3%. As in the GEP(2) experiment, the polarization components for the background will be measured with a precision higher that for the elastic events. Therefore, the corresponding corrections to the form factor ratio will result in a negligible systematic error.

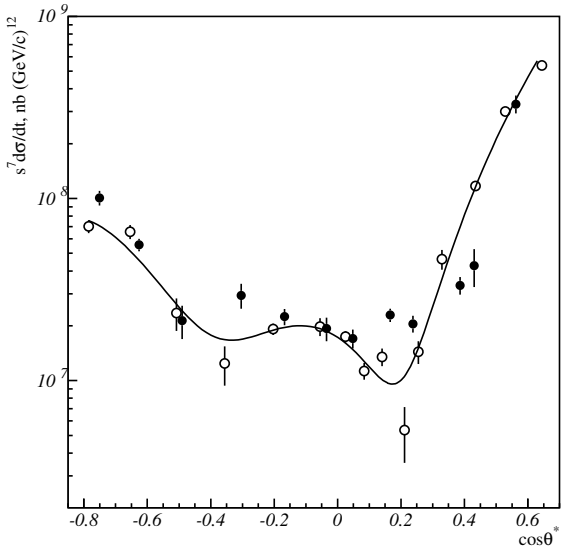

Figure 24: Invariant cross-section times s^7 of the $\gamma p \to \pi^0 p$ reaction for gamma energies of 4 GeV (open circles) and 5 GeV (solid circles) [87].

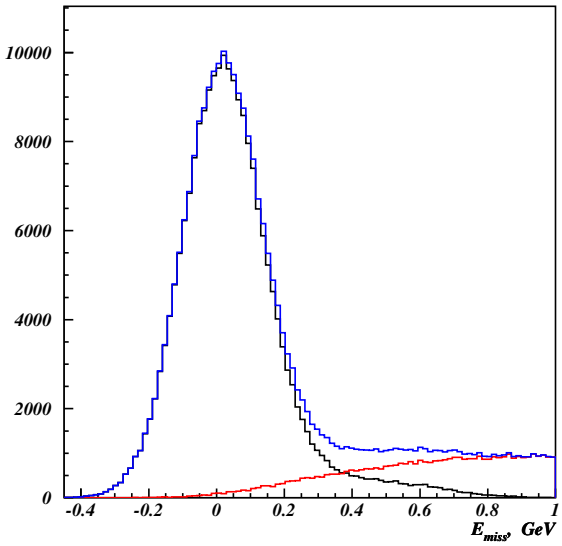

Figure 25: Missing energy (E_{miss}, difference between the calorimeter energy and the one expected from the proton arm for elastic kinematics) spectra of the elastic (black), π^0 photoproduction (red), and their sum (blue). To reject the inelastic events a cut is applied for $E_{miss} > 0.35$ GeV.

8 Proposed measurements

8.1 Production measurements

We propose to measure the proton form factor ratio G_{Ep}/G_{Mp} in the Q^2 interval of 12.3−16.0 $(GeV/c)^2$ in a single detector setting with one beam energy of 11 GeV for 56 days. The statistics will be subdivided into two intervals $12.3-13.5$ and $13.5-16.0$ $(GeV/c)^2$ resulting in two data points at Q^2 of 12.9 and 14.8 GeV^2. In addition we propose a control measurement at Q^2 of 6.24 $(GeV/c)^2$ using a beam energy of 4.4 GeV without moving the proton arm.

The kinematical quantities for these points are summarized in Table 3.

Q^2 $(GeV/c)^2$	E_e GeV	θ_e deg	$E_{e'}$ GeV	θ_p deg	p_p GeV/c
6.24	4.4	70.11	1.08	14.1	4.16
12.90	11.	30.92	4.13	15.9	7.75
14.75	11.	38.14	3.14	12.8	8.75

Table 3: The kinematics of the proposed data points.

The rate estimates, and the Figure-of-Merit extrapolated to the high momentum region as desribed in Section 5.3, are shown in Table 4.

Q^2 $(GeV/c)^2$	$d\sigma/d\Omega_e$ cm^2/sr	$d\Omega_e$ msr	rate Hz	ϵA_y^2 FOM
6.24	8.2×10^{-37}	188	117	3.61×10^{-3}
12.90	1.7×10^{-37}	35	4.19	1.04×10^{-3}
14.75	4.2×10^{-38}	127	4.25	0.82×10^{-3}

Table 4: Expected event rates and Figure-of-Merit.

The anticipated errors of the proposed points are given in Table 5 and shown in Fig.26. We are assuming a beam of 75 μA intensity, and 85 % beam polarization. In these calculations we use the size of the target for which there is a full aceptance for the given Q^2 region, which is 40 cm for the 6.24 and 14.75 GeV^2 points, and 35 cm for the 12.90 GeV^2 point. For all the kinematics the calorimeter is at a distance of 3.5 m. It matches the proton arm solid angle for the high Q^2 measurements, and reduces it by a factor 2.6 for the control measurements.

Q^2 $(GeV/c)^2$	beam time days	$\Delta[\ \mu G_E/G_M]$ stat.
6.24	2	0.037
12.90	for both	0.088
14.75	56	0.105

Table 5: Proposed data points and anticipated statistical uncertainty.

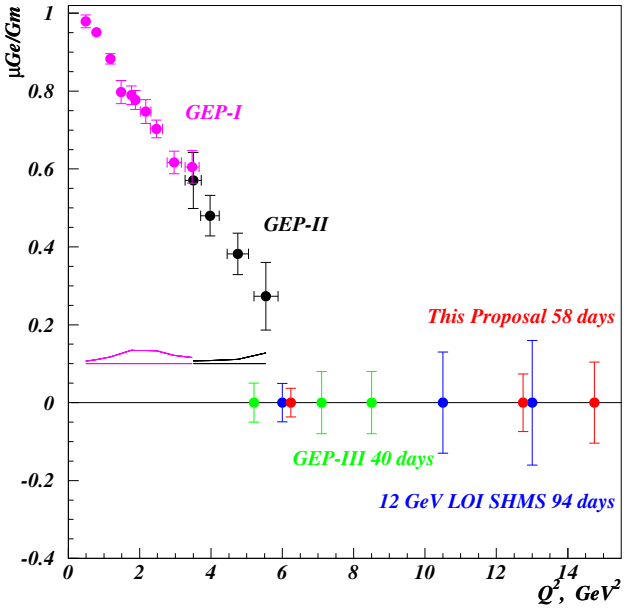

Figure 26: The proposed data points.

8.2 Calibration of the proton arm and its optics

The magnetic system of the proton arm is very simple in the proposed experiment. It consists of a single dipole magnet (48D48). For the present plan we are going to use only the central 60% of the magnet gap, so effects of the fringe field near the edges are reduced even more. Nevertheless, to minimize the systematic effects we plan to check the deflection in the non-dispersive plane by turning the magnet on and off. Compared to the previous GEP experiments, such task is mach easier here because of the direct view of the target from the tracking chambers.

For the optical studies we will use electrons scattered from the carbon target. Several thin carbon foils will be installed in beam with 4 cm spacing. The sieve slit will be used to define the scattering angle of the electrons. The calibration of energy reconstruction will be done by using elastic scattering events with the recoil proton detected at 32° in BigCal, and the electron in the proton arm. The large cross section for such inverse measurement leads to a 100 Hz rate of elastic *ep* events even with 10 times lower luminosity. Scattered electrons of 8 GeV momentum match the momentum of proton in production run. Total time for optics commissioning is estimated in 16 hours, which is included in the experiment beam time budget.

8.3 Beam time request

The beam time request for the proposed experiment is summarized in Table 6. High degree of beam polarization is very important, so we plan to do a spin "dance" to insure maximum logitudinal polarization.

Item	Beam energy GeV	Q^2 $(GeV/c)^2$	Beam time hours
Optics	4.4		24
Production	4.4	6.24	48
Spin study	11.0		24
Production	11.0	12.9 & 14.8	1344
Total			1440

Table 6: Beam time request. Total budget is 60 days.

9 Summary

We request 60 days of beam time to measure G_{Ep}/G_{Mp} at $Q^2 = 12.9$ and 14.8 $(\mathrm{GeV/c})^2$ through a measurement of the polarization transfer in the elastic reaction $H(\vec{e}, e'\vec{p})$. We propose to measure G_{Ep}/G_{Mp} to an absolute statistical accuracy, $\Delta[\mu_p G_{Ep}/G_{Mp}] \sim 0.1$, which would match the precision achieved in lower momentum transfer recoil polarization measurements at JLab, (GEP(1) and GEP2)). This experiment will be done in Hall A, and will utilize BigCal to detect electrons scattered off a 40 *cm* cryogenic target, and a customized setup for detecting the recoil proton which will include a dipole magnet, three new fast trackers for the determination of its momentum, interaction vertex and polarization, as well as a hadron calorimeter to control the trigger rate. The dipole, type 48D48, is available from the fixed target AGS program at BNL. The polarimeter can be developed from the existing new polarimeter built for GEP(3) in Hall C. Several options exist for the hadron calorimeter. One likely option is to reuse parts of calorimeters that exist at several collaborating institutions. The new and key part of the detector is the set of tracking chambers; these are conceptually similar to ones used in the COMPASS experiment at CERN.

Knowledge of the proton form factors is crucial for the understanding of the structure of the nucleon. Form factor data are required for tests of QCD. Recent results from lattice QCD calculations have become sufficiently accurate to allow for direct comparison with data. Phenomenological models have been challenged by elastic form factor data obtained at Jefferson Lab. The Pauli form factor F_2 provides a unique way to determine the Generalized Parton Distribution $E(x, \xi, t)$, which is not accessible from DIS data; F_2 is a convolution over x of $E(x, \xi, t)$. Another proposal to this PAC [91] will access the ep elastic cross section with the goal of re-measuring G_{Mp} to better accuracy than done in the past; it will require the G_{Ep}/G_{Mp} ratio to extract G_{Mp} from cross sections. In addition, form factors at the largest possible Q^2 are a necessary input in the analysis and interpretation of the quark orbital angular momentum in the nucleon. It is of course also an intriguing question whether the G_{Ep}/G_{Mp} ratio will become negative and what is the physics responsible for it.

10 Coordination of GEP(4) and GEP(5)

The LOI 12-06-103 submitted to PAC 30 described an experiment utilizing the super HMS to measure the G_{Ep}/G_{Mp} ratio up to 13 GeV^2. It was well received by the PAC and the collaboration is planning to submit a full proposal to PAC 34. This experiment will use existing equipment, including the focal plane polarimeter recently built for GEP(3), and the calorimeter BigCal likewise built for the same experiment. It will therefore require very small laboratory resources to run, beyond the new standard equipment in Hall C (the superHMS). However, due to the small solid angle of the super HMS (3.5 mr), the predicted error bar is 0.16 at 13 GeV^2, to be obtained in 60 days of beam on target. We see two reasons the two proposals, this one and the future GEP(4), should be considered complementary. GEP(5) is submitted before GEP(4) for "strategic" reasons: it requires early funding for new instrumentation, and time for construction; GEP(4) can use the standard equipment in Hall C very soon after the 11 GeV upgrade.

1) the mapping of the form factor ratio in the region of Q^2 above 9 GeV^2 is of great interest. GEP(3) will probably be limited to 8.5 GeV^2 because of insufficient beam energy. Having new data points at 10.5, 13 and 15 GeV^2, 13 GeV^2 being an overlap point between the 2 experiments, is very reasonable: we known from GEP(2) that reduction of the pion generated background, which can simulate elastic *ep* events, is crucial for obtaining the correct form factor ratio; the backgrounds will definitively be different in the 2 experiments.

2) The GEP collaboration has been instrumental in developing the recoil polarization technique at JLab; in particular it has initiated calibration measurements in Dubna, which have been determinant in getting GEP(3) approved. We have an approved project to continue these calibrations in Dubna in 2008/9, with the goal of reaching a proton momentum 8 GeV/c; there is presently absolutely no information for the analyzing power of either carbon or CH_2 at such proton momenta; the existing data for *pp* elastic scattering can only be used as an indication that the analyzing power will not be too small to be usable.

11 Collaboration responsibilities and expected stages of development

The following is a list of personnel from the institutions and their intended contribution to the proposed experiment:

- The William and Mary PI and collaborators of this experiment are committed to implement upgrade and operation support of the BigCal calorimeter. They will also take responsibility for implementation of the hadron calorimeter in this experiment. The source of funding for this group is NSF.
- The Norfolk State University PI and collaborators for this experiment will use their expertise in tracking detectors to contribute to aspects of DAQ and the GEM trackers. The source of funding for this group is DOE.
- The INFN group consists of 3 faculty members in Rome and 2 in Bari, as well as two research scientists and one post-doc committed to this experiment. The source of research funding for this group is the INFN. This group intends to contribute at least 7 FTE-years. The group has recently constructed a large RICH counter for the HRS in Hall A, and will take a leading role in development and construction of the trackers for this experiment.
- The Hall A contribution will be the infrastructure for the 48D48 magnet, consisting of the carriage for installation of the magnet in Hall A, and modification of the control for the power supply (which will be provided by BNL, together with the dipole magnet).

Below is a preliminary plan of the development for the proton arm:
The INFN group is organizing several institutions in this collaboration to coordinate different aspects of the GEM base trackers. These groups are INFN(Rome), INFN(Bari), Norfolk State University, MIT, Glasgow University, Florida International University, and UVA. We expect that a small scale prototype GEM-based chamber will be constructed in early 2008 and could be used in Hall A for rate measurements, and in HRS optics studies. Depending on the funding profile for 2008/9, the INFN group has set a goal of construction of the larger trackers (with dimensions of 30x140 cm^2), such that they can be tested in the BigBite spectrometer in 2009. Depending on funding availability, the INFN group **intends** to contribute about 33% of the resources required to build the tracking system for this proposal.

The Glasgow group **intends** to work on similar GEM-based detectors for the PANDA experiment and will share their results in hardware design and readout software with this experiment, effectively contributing several FTE's.

The Florida International University also **intends** to contribute in the development of a GEM-based tracker at least 1 FTE and put a graduate PhD thesis student in this experiment.

The University of Virginia group, which recently developed a major new tracker for the BigBite spectrometer, **intends** to contribute at least 1 FTE to the development of a GEM-based tracker.

The College of William and Mary group, together with Dubna collaborators, **intends** to prepare the hadron calorimeter elements and their implementation in time for the experiment

around 2012. These two groups will also undertake an (approved) experiment with a ~ 8 GeV/c polarized proton beam at the Dubna Nuclotron, to measure the analyzing power and efficiency of a polarimeter similar to the one required for this proposal. This experiment will also test the use of the hadron calorimeter as part of the trigger, including study of selectivity of the elastic process of the analyzing reaction on CH_2.

The Carnegie Mellon University group and Hall A are preparing a proposal to measure magnetic form factor of the neutron (with 6 GeV beam) which will be submitted to PAC33. A key new element of that proposal is the deflection magnet 48D48 required for the present proposal. These two groups **intend** to join efforts in the preparation of the 48D48 magnet for the present proposed experiment.

The Yerevan (Armenia) group and Protvino groups (Russia) **intend** to continue operational support for the electromagnetic calorimeter BigCal.

The proposed magnet-detector system of the proton arm provides a unique new resource for future Hall A experiments, such as the semi-inclusive electron scattering from different polarized targets, neutron electric form factor measurements, and J/Ψ photo-production.

References

[1] G.A. Miller, *Phys. Rev.* **C68** (2002) 022201(R).

[2] M. Burkardt, Phys. Rev. **D66**, 114005 2002.

[3] X. Ji, *Phys. Rev.* **D55** (1997) 7114, *Phys. Rev. Lett.* **78**, (1997) 610.

[4] A.V. Afanansev *et al.*, Phys Lett. **B514**, 269 (2001).

[5] O. Gayou *et al.*, *Phys. Rev. Lett.* **88**, 092301 (2002).

[6] V. Punjabi *et al.*, *Phys. Rev.* **C71**, 055202 (2005), [Erratum-ibid. **C71**, 069902 (2005)].

[7] J. Arrington, *Phys. Rev.* **C68**, 034325 (2003).

[8] O. Gayou *et al.*, *Phys. Rev.* **C64**, 038202 (2001).

[9] G.A. Miller, arXiv:0705.2409 (2007).

[10] L. Andivahis *et al* Phys. Rev. **50**, 5491 (1994).

[11] M. E. Christy *et al*, Phys. Rev. C **70**, 015206 (2004).

[12] I.A. Qattan *et al*, Phys. Rev. Lett. **94**, 142301 (2005).

[13] F. Iachello, A.D. Jackson, and A. Landé, *Phys. Lett.* **B43**, 191 (1973).

[14] G. Höhler *et al.*, Nucl. Phys. **B114**, 505 (1976).

[15] M.F. Gari and W. Kruempelmann, Z. Phys. **A322**, 689 (1985) 689; M.F. Gari and W. Kruempelmann, Phys. Lett. **B274**, 159 (1992); M.F. Gari and W. Kruempelmann, Phys. Lett. **B282**, 483(E) (1992).

[16] P. Mergell, U.G. Meissner, and D. Drechsel, Nucl. Phys. **A596**, 367 (1996).

[17] H.-W. Hammer and Ulf-G. Meissner, Eur. Phys. J. **A20**, 469 (2004).

[18] E.L. Lomon, *Phys. Rev.* **C64**, 035204 (2001).

[19] F. Iachello and Q. Wan, *Phys. Rev.* **C69**, 055204 (2004).

[20] R. Bijker and F. Iachello, *Phys. Rev.* **C69**, 068201 (2004).

[21] M.A. Belushkin, H.W. Hammer and U.G. Meissner, *Phys. Rev.* **C75**, 035202 (2007).

[22] G. Holzwarth, Z Phys. **A356**, 339 (1996); G. Holzwarth, hep-ph/0201138 v1 (2002).

[23] P. l. Chung and F. Coester, *Phys. Rev.* **D44**, 229 (1991).

[24] I.G. Aznauryan, Phys. Lett. **B316**, 391 (1993).

[25] Z. Dziembowski *et al.*, Ann. of Phys. **258**, 1 (1997).

[26] M.R. Frank, B.K. Jennings, and G.A. Miller, *Phys. Rev.* **C54**, 920 (1996).

[27] F. Cardarelli, E. Pace, G. Salme and S. Simula, Phys. Lett. **B357**, 267 (1995).

[28] M. De Sanctis, M.M. Giannini, L. Repetto and E. Santopinto, *Phys. Rev.* **C62**, 25208 (2000).

[29] S. Boffi *et al.*, Eur. Phys. J. A **14**, 17 (2002); S. Boffi *et al.*, hep-ph/0108271 v1 (2001).

[30] F. Gross and P. Agbakpe, nucl-th/0411090 v1 (2004).

[31] J. Friedrich and Th. Walcher, Eur. Phys. J. **A17**, 607 (2003).

[32] D.H. Lu, A.W. Thomas and A.G. Williams, *Phys. Rev.* **C57**, 2628 (1998).

[33] P. Kroll, M. Schurmann and W. Schweiger, Z. Phys. **A338**, 339 (1991).

[34] B.Q. Ma, D. Quing and I. Schmidt, *Phys. Rev.* **C65**, 035205 (2002).

[35] A.V. Radyushkin, Acta Phys. Polnica **B15**, 40 (1984).

[36] D.B. Leinweber, A.W. Thomas, R. D. Young, *Phys. Rev. Lett.* **86** (2001) 5011.

[37] C. Alexandrou, G. Koutsou, J.W. Negele, A. Tsapalis, *Phys. Rev.* **D74** (2006) 034508.

[38] M. Göckeler, *et al.*, QCDSF/UKQCD Collaboration, PoS LAT2006 (2006) 120. arXiv:hep-lat/0610118.

[39] R.G. Edwards, *et al.*, LHPC Collaboration, arXiv:hep-lat/0610007.

[40] D. Müller, D. Robaschik, B. Geyer, F.M. Dittes, J. Horejsi, Fortsch. Phys. 42 (1994) 101.

[41] A.V. Radyushkin, *Phys. Lett.* bf B380 (1996) 417.

[42] X.D. Ji, *J. Phys.* **G24** (1998) 1181.

[43] K. Goeke, M.V. Polyakov, M. Vanderhaeghen, Prog. Part. Nucl. Phys. 47 (2001) 401.

[44] Diehl M., Phys. Rept. 388 (2003) 41.

[45] X. Ji, Ann. Rev. Nucl. Part. Sci. 54 (2004) 413.

[46] A.V. Belitsky, A.V. Radyushkin, Phys. Rept. 418 (2005) 1.

[47] S.J. Brodsky, G.R. Farrar, *Phys. Rev.* **D11**, (1975) 1309.

[48] V.L. Chernyak, A.R. Zhitnitsky, JETP Lett. 25 (1977) 510; Pisma Zh. Eksp. Teor. Fiz. 25 (1977) 544.

[49] V.L. Chernyak, A.R. Zhitnitsky, V.G. Serbo, JETP Lett. 26 (1977) 594; Pisma Zh. Eksp. Teor. Fiz. 26 (1977) 760.

[50] A.V. Efremov, A.V. Radyushkin, *Phys. Lett.* **B94** (1980) 245.

[51] G.P. Lepage, S.J. Brodsky, *Phys. Rev.* **D22**, (1980) 2157.

[52] W.K. Brooks and J.D. Lachniet [CLAS Collaboration], Nucl. Phys. **A755**, 261 (2005), and J.D. Lachniet, PhD thesis, Carnegie Mellon Univesity, unpublished (2005)

[53] A. De Rujula, H. Georgi and S.L. Glashow, *Phys. Rev.* **D12**, 147 (1975); N. Isgur and G. Karl, *Phys. Rev.* **D18**, 4187 (1978); **19**, 2653 (1979); **20**, 1191 (1979); C. Hayne and N. Isgur, *ibid* **25**, 1944 (1982).

[54] F. Schlumpf, *Phys. Rev.* **D47**, 4114 (1993); J. Phys. **G20**, 237 (1994).

[55] G.A. Miller and M.R. Frank, *Phys. Rev.* **C65**, 065205 (2002).

[56] M.K. Jones *et al.*, *Phys. Rev. Lett.* **84**, 1398 (2000).

[57] F. Cardarelli and S. Simula, *Phys. Rev.* **C62**, 65201 (2000).

[58] M. Guidal, M. V. Polyakov, A. V. Radyushkin, and M. Vanderhaeghen, *Phys. Rev.* **D72**, 054013 (2005).

[59] E. Brash, M.K. Jones, C.F. Perdrisat and V. Punjabi, GEP-III, JLab Experiment 04-108 (2004).

[60] T. Janssens, R. Hofstadter, E.B. Hughes and M.R. Yearian, *Phys. Rev.* **142**, 922 (1966).

[61] J. Litt *et al.*, *Phys. Lett.* **B31**, 40 (1970).

[62] Ch. Berger *et al.*, *Phys. Lett.* **B35**, 87 (1971).

[63] W. Bartel *et al.*, Nuc. Phys. B **58**, 429 (1973).

[64] R.G. Arnold *et al.*, *Phys. Rev. Lett.* **57**, 174 (1986); A.F. Sill *et al.*, *Phys. Rev.* **D48**, 29 (1993).

[65] E.J. Brash, A. Kozlov and G.M. Huber, *Phys. Rev.* **C65**, 051001 (2002).

[66] C.B. Crawford, *et al.*, arXiv:nucl:ex/0608007.

[67] A.V. Belitsky, Xiandong Ji and Feng Yuan, *Phys. Rev. Lett.* **91**, 092003 (2003).

[68] J.P. Ralston and P. Jain, *Phys. Rev.* **D69**, 053008 (2004).

[69] S.J. Brodsky, J.R. Hiller, D.S. Hwang and V.A. Karmanov, *Phys. Rev.* **D69**, 076001 (2004).

[70] H.H. Matevosyan, A.W. Thomas and G.A. Miller, *Phys. Rev.* **C72**, 065204 (2005); *Phys. Rev.* **C71**, 055204 (2005).

[71] A.I. Akhiezer and M.P. Rekalo, Sov. J. Part. Nucl.**3**, 277 (1974).

[72] R. Arnold, C. Carlson, and F. Gross, *Phys. Rev.* **C23**, 363 (1981).

[73] C.F. Perdrisat, V. Punjabi, M.K. Jones, and E. Brash, JLab PAC20 proposal 01-109 (2001); C.F. Perdrisat, V. Punjabi, M.K. Jones, and E. Brash, JLab PAC26 update 04-108 (2006).

[74] L.S. Azhgirei *et al.*, *Nucl. Instr. Meth.* **A538**, (2005) 431.

[75] I.M. Sitnik, *Nucl. Instr. Meth.* **A527**, (2004) 278.

[76] H. Spinka *et al.*, *Nucl. Instr. Meth.* **A211**, 239 (1983).

[77] L. Pentchev, JLAB-TN-03-024 (2003).

[78] N.E. Cheung *et al.*, *Nucl. Instr. Meth.* **A363** (1995) 561.

[79] I.A. Alekseev *et al.*, *Nucl. Instr. Meth.* **A434**, 254 (1999).

[80] E. Brash, M.K. Jones, C.F. Perdrisat and V. Punjabi, JLab 12 GEV PAC30, LOI (2006).

[81] F. Sauli, *Nucl. Instr. Meth.* **A386** (1997) 531.

[82] R. Chechik *et al.*, *Nucl. Instr. Meth.* **A535** (2004) 303.

[83] B. Ketzer *et al.*, *Nucl. Instr. Meth.* **535** (2004) 314.

[84] N.V. Vlasov *et al.*, Instruments and Experimental Techniques **49** (2006) 41.

[85] A.M. Boyarski *et al.*, *Phys. Rev.* **D14**, 1733 (1976).

[86] V.A. Matveev, R.M. Muradyan and A.N. Tavkhelidze, *Lett. Nuovo Cimento* **7**, 719 (1973); S.J. Brodsky and G. Farrar, *Phys. Rev. Lett.* **31**, 1153 (1973).

[87] R.L. Anderson *et al.*, *Phys. Rev.* **D14**, 679 (1976).

[88] A. Danagulian *et al.*, *Phys. Rev. Lett.* **98**, 152001 (2007).

[89] A. Shahinyan *et al.*, arXiv:0704.1830 [physics.ins-det].

[90] C.F. Perdrisat, V. Punjabi, M. Vanderhaeghen, arXiv:hep-ph/0612014.

[91] S. Gilad, B. Moffit, J. Arrington and B. Wojtsekhowski, "Precision Measurement of the Proton Elastic Cross Section at High Q^2", PAC 32 proposal, 2007.